ONE DIMENSIONAL TiO_2 PREPARATION AND DYE-SENSITIZED SOLAR CELL APPLICATIONS

MS. METHAWEE NUKUNUDOMPANICH
ID: 56300700508

A THESIS SUBMITTED AS A PART OF THE REQUIREMENTS FOR THE DEGREE OF MASTER OF ENGINEERING IN ENERGY TECHNOLOGY AND MANAGEMENT

THE JOINT GRADUATE SCHOOL OF ENERGY AND ENVIRONMENT AT KING MONGKUT'S UNIVERSITY OF TECHNOLOGY THONBURI

2ND SEMESTER 2014

One Dimensional TiO_2 Preparation and Dye-Sensitized Solar Cell Applications

Ms. Methawee Nukunudompanich
ID: 56300700508

A Thesis Submitted as a Part of the Requirements
for the Degree of Master of Engineering
in Energy Technology and Management

The Joint Graduate School of Energy and Environment
at King Mongkut's University of Technology Thonburi

2nd Semester 2014

Thesis Committee

.....	
(Assoc. Prof. Dr. Jatuphorn Wootthikanokkhan)	Advisor
.....	
(Dr. Surawut Chuangchote)	Co-Advisor
.....	
(Assoc. Prof. Dr. Yoshikazu Suzuki)	Member
.....	
(Asst. Prof. Dr. Sorapong Pavasupree)	Member
.....	
(Asst. Prof. Dr. Yutaka Shinoda)	External Examiner

Thesis Title: One Dimensional TiO_2 Preparation and Dye-sensitized Solar Cell Applications

Student's name, organization and telephone/fax numbers/email

Miss Methawee Nukunudompanich

The Joint Graduate School of Energy and Environment (JGSEE)

King Mongkut's University of Technology Thonburi (KMUTT)

126 Pracha Uthit Rd., Bangmod, Tungkru, Bangkok 10140 Thailand

Telephone: 0-8408-72200

Email: mintmonster2@gmail.com

Supervisor's name, organization and telephone/fax numbers/email

Assoc. Prof. Dr. Jatuphorn Wootthikanokkhan

School of Energy, Environment and Materials

Division of Materials Technology,

King Mongkut's University of Technology Thonburi (KMUTT)

126 Pracha Uthit Rd., Bangmod, Tungkru, Bangkok 10140 Thailand

Telephone: 0-2470-8693-99 to 316 Fax: 0-2427-9062

E-mail Address: jatuphorn.woo@kmutt.ac.th

Co-Advisor's name, organization and telephone/fax numbers/email

Dr. Surawut Chuangchote

The Joint Graduate School of Energy and Environment (JGSEE)

King Mongkut's University of Technology Thonburi (KMUTT)

126 Pracha Uthit Rd., Bangmod, Tungkru, Bangkok 10140 Thailand

Telephone: 086-388-0493 Fax: 02-8726736

E-mail Address: surawut.chu@kmutt.ac.th

Topic: One Dimensional TiO_2 Preparation and Dye-sensitized Solar Cell Applications
Name of Student: Miss Methawee Nukunudompanich **Student ID:** 56300700508
Name of Supervisor: Assoc. Prof. Dr. Jatuphorn Wootthikanokkhan
Name of Co-Advisor: Dr. Surawut Chuangchote

ABSTRACT

Dye-sensitized solar cells (DSSC) are expected to substitute for silicon solar cells due to its lower costs. Most general electrodes used in DSSCs are fabricated with interconnected TiO_2 nanoparticles that contain large surface areas for adsorbing dye molecules and acting as electron transportation pathways. However, the random contacts among TiO_2 nanoparticles form grain boundaries, leading to trapping and recombination of electrons with holes, andlimits the efficiency of the DSSCs. Alternatively, TiO_2 nanowires, i.e. nanorods or nanotubes, have been proposed as ~~a~~ promising materials for the working electrode due to its large surface area and high electron transportation capability through the TiO_2 nanowires. Among various synthesis methods, anodic aluminum oxide template method (AAO) is one that the film with uniform one-dimensional (1-D) pore channels is used as a template for nanowires. This method is adaptable for applicability and uniformly ordered structure. In this research, changing the AAO hole diameter (100 and 200 nm) of the nanorods and the semi-nanotubes were synthesized by simple ways, *i.e.* immersion setting (nanorods) and vacuum and drop setting (nanowire)~~.~~ The synthesized nanorods or semi-nanotubes were mixed with commercial TiO_2 nanoparticles (P-25, PlasmaChem GmbH) with mixing ratios of 5:95, 10:90 and 15:85 (by mass) and then utilized as photoelectrode of DSSCs. The optimum mixing ratios for the nanorods and the semi-nanotubes are 5:95 and 10:90, respectively. The DSSCs with photoelectrodes made using the nanorods or the semi-nanotubes showed better performances than those with electrodes made using only TiO_2 nanoparticles, because of the effects of one-dimensional (1-D) nanostructure.

Keywords: Anodic aluminum oxide (AAO), Dye-sensitized solar cell (DSSC), TiO_2, Nanorod, Nanotube.

ACKNOWLEDGEMENTS

I would like to acknowledge several people who kindly helped and supported.

Firstly, I would like to acknowledge my advisor, **Assoc. Prof. Dr. Jatuphorn Wootthikanokkhan**. He always answered my questions and a lot of effort into my thesis. I will remember his helpfulness. Thank you very much.

Secondly, I would like to acknowledge **Assoc. Prof. Dr. Yoshikazu Suzuki** (Suzuki sensei) for guiding me during my exchange research in Japan. I would especially like to thank Suzuki sensei for being my unofficial second advisor. Although I was not his official student, he always treated me as if I were one. He invited me to Suzuki's Group meetings and conferences. He supported my researches by allowing me to use all instruments in his laboratory. I was a member of his research groups and he freely gave me advice. I can honestly say Suzuki sensei inspires me to fight for science. I am very grateful for the time he has dedicated to me, his suggestions, and useful discussions. Thank you also for the friendly environment in which his laboratory has welcomed me. Without him and his colleagues, I would be alone in Japan. So, I thought I have found the second home in Japan. All of these have been of great supports, helping me to face the ups and downs of my thesis, which I do not think I would have completed it otherwise. Thank you for not only experiment but also all experience I got from Japan.

Thirdly, I would like to thank **Dr. Surawut Chuangchote**. He always stood by me for many times. He gives me wonderful ideas and guides me many steps of my experiments to success. He often advises me about thesis writing and thesis presentation and makes them better. Thanks for always support and cheer me up. From the bottom of my heart I would like to thank Dr. Surawut for believing in me and being my advisor for me through some of the best and worst times of my master degree.

Fourthly, I would like to thank my friends (JGSEE, Tsukuba, UNC, and every other great person). They were always besides me. We always solve many problems together and travel to many places together. They never would let me fall and always cheer me up. Thank you very much my friends.

Next, this work is the result of collaborations within different universities and other research institutes. I would like to express my gratitude to:

The University of Tsukuba for giving me a chance to do research with them and supporting for the grant for international research program;

Asst. Prof. Dr. Yutaka Shinoda, Tokyo Institute of Technology, for his help on SEM observations; and

The Joint Graduate School of Energy and Environment for financially supporting for research.

Finally, I would like to thank my family. They supported me every time I felt like giving up or tiring and stood always beside me when I have problems. Thank you very much, my beloved family.

CONTENTS

CONTENTS (Cont')

CONTENTS (Cont')

LIST OF FIGURES

LIST OF FIGURES (Cont')

LIST OF FIGURES (Cont')

LIST OF FIGURES (Cont')

LIST OF TABLES

LIST OF ABBREVIATIONS

J = Output current density (A/Cm^2)

V = Voltage (V)

J_{ph} = Photocurrent density (A/Cm^2)

J_0 = Reverse saturation current density (A/Cm^2) of diode

K = The Boltzmann constant ($1.3806488 \times 10^{-23}\ M^2\ Kg\ S^{-2}\ K^{-1}$)

Q = Electron charge

T = Absolute cell temperature

N = Diode ideality factor

R_S = Specific series

R_{sh} = Shunt resistances (Ω/Sq.)

FF = Fill Factor

PCE = Power conversion efficiency

AAO = Anodic aluminium oxide

IS = Immersion setting

VDS = Vacuum drop setting

NR = Nanorod

NP = Nanoparticle

SNT = Semi-nanotubes

SEM = Scanning electron microscopy

XRD = X-ray diffraction

EDS = Energy dispersion spectroscopy

UV-vis = Ultraviolet-visible

CHAPTER 1

INTRODUCTION

1.1 Rational

O'Regan and Grätzel were the first to report on the low-cost dye-sensitized solar cells (DSSCs) in 1991 [1]. DSSC was expected to be a candidate complementary to the silicon solar cells, due to DSSCs being cheaper inexpensiveness and simpler in manufacturing processes. The highest efficiency among the DSSCs was achieved by the combination of liquid electrolyte and titanium oxide (TiO_2) as a working electrode, which demonstrates overall light-to-electricity conversion efficiencies over 12% [2-6]. The most general electrode used in DSSCs is fabricated with interconnected TiO_2 nanoparticles which contain large surface area for adsorbing dye molecules and act as electron transportation pathway [4, 7]. While the dye molecules on the TiO_2 nanoparticles absorbed photons from light, a current is produced by electron injection from dye travels to the conduction band of TiO_2. As a result the electrons transport through the TiO_2 nanoparticles to arrive at the electrode. However, the random contacts among TiO_2 nanoparticles form grain boundaries leading to trapping and recombination of electrons with holes, which limits the efficiency of the DSSCs [4, 8-9].

Although, TiO_2 nanotubes derived from nanoparticles by solution processes have been proposed as a promising material for the working electrode with an ordered structure, due to its large surface area, and high electron transportation capability through the ordered TiO_2 nanotubes, the DSSCs made with the nanotubes still do not exhibit more efficient performance than those with the TiO_2 nanoparticles because their thermal stability is generally poor and they easily fragment into nanoparticles at a temperature around 500-600˚C, which is nearly the sintering temperature of the electrode (around 500 ˚C) [7]. Significant attempts have been made to develop one-dimensional (1-D) nanostructured materials [7-8, 10-12]. In these materials, greater photovoltaic performances may be attained through the understanding of anode materials with the improvement of electron transport capability [4, 12-13]. TiO_2 nanowires, i.e. nanorods or nanotubes, are primarily interesting candidates to achieve this purpose [4, 7, 14]. There have been various methods to grow up TiO_2 nanostructures, including sol-gel process, electrospinning, and anodization of Ti metal [10-11, 14]. However, these methods have limitations in synthesizing uniform TiO_2 nanorods or nanowires having ordered structures with accurate control of dimension and geometry [15, 16] that strongly influence the diffusion of

excitons and the conduction of electrons, and consequently affect overall power conversion efficiency (PCE) of the DSSCs [17].

Anodic aluminum oxide (AAO) template method is a synthesis process in which AAO film with uniform 1-D pore channels is used as a template for a 1-D nanostructure. AAO template method is suitable to prepare TiO_2 nanorods and nanowires with uniformly ordered structures. Just by changing a hole diameter and thickness of AAO or infiltration depth of precursor into AAO, size and aspect ratio of 1-D nanomaterials can be easily controlled [16-19]. Therefore, in this study, AAO containing 100 and 200 nm pores were used as templates to prepare 1-D nanostructured TiO_2. The aim of this work is to control the diameter and shape of the nanostructured TiO_2, i.e. nanorods and semi-nanotubes, by the AAO template method. The AAO template was eventually removed by NaOH aq. treatment). The obtained nanorods or semi-nanotubes were utilized as photoelectrodes in DSSCs. The sonication followed by magnetic stirring mixing was used for better dispersion. To reduce crack formation on the surface, the photoanodes were coated 2 times.

1.2 Literature Review

1.2.1 Dye sensitized solar cells (DSSCs)

B. Liu and E. S. Aydil [12] studied a hydrothermal method to grow oriented, single-crystalline rutile TiO_2 nanorod films on transparent conductive fluorine-doped tin oxide (FTO) glasses. The diameter, length, and density of the nanorods were varied by changing the growth parameters such as growth time, growth temperature, reactant concentration, acidity and additives. The small lattice mismatch between the FTO substrate and rutile TiO_2 plays a key role in driving the nucleation and growth of the rutile TiO_2 nanorods on FTO. With $TiCl_4$-treatment, a light-to-electricity conversion efficiency of 3% could be achieved by using TiO_2 nanorod films as the photoanode in a DSSC.

K. Asagoe *et al.* [7] prepared TiO_2 (B) and TiO_2 anatase nanowires by a hydrothermal method. TiO_2 (B) is a metastable polymorph of TiO_2, Although, the first synthesized DSSC with fully nanowire electrodes showed a low light-to-electricity power conversion efficiency (*PCE*) around 1.33 % for TiO_2 (B) and 2.42% for TiO_2 anatase, (10 wt%) nanowire-dispersed electrodes in TiO_2-nanoparticle matrixes improved efficiency up to 6.17 % for TiO_2 (B) and 6.53% for TiO_2 anatase. These *PCEs* were higher than that of the cell made of pure nanoparticle electrodes in this work (*PCE* = 5.59%).

D. Kuang *et al*. [8] fabricated TiO_2 nanotube arrays by electrochemical anodization of Ti foils, which showed excellent light to electricity conversion efficiency in the DSSCs. A flexible DSSC using TiO_2 nanotube arrays on a Ti foil as a working electrode and indium tin oxide/polyethylene naphthalate (ITO/PEN) as a counter electrode in combination with solvent-free ionic liquid electrolyte achieved 3.6% *PCE*.

Y. Suzuki *et al* [4] prepared partially nanowire-structured TiO_2 by a hydrothermal processing followed by calcinations in air. A DSSC with a film thickness of 5.6 μm, fabricated using the partially nanowire-structured TiO_2 showed better performance than did using a conventional equiaxed TiO_2 nanoparticles. The short-circuit current density (J_{sc}), the open-circuit voltage (V_{oc}), the fill factor (*FF*), and *PCE* are 11.9 mA/cm^2, 0.754 V, 0.673 and 6.01 %, respectively.

Y. Wang *et al*. [20] reported that oriented ZnO nanowire-covered TiO_2 nanoparticle composite film electrodes were fabricated by screen-printed TiO_2 nanoparticle layers on conducting glass and low-temperature hydrothermal growth of ZnO nanowires. DSSCs based on the composite electrode gained J_{sc} of 8.04 mA/cm^2, V_{oc} of 0.67 V, *FF* of 0.40, and overall conversion efficiency of 2.15%.

Q. Hu *et al*. [14] synthesized TiO_2 nanowires by hydrothermal treatment and the composite photoanodes were prepared through mixing various mass ratios of nanowires and nanoparticles. DSSC with PW10 (nanowires content was 10 wt %) photoanode showed a relative high conversion efficiency of 6.27% because of the synergistic role of the high specific area of nanoparticles and rapid electron transfer of nanowires.

J. Wang *et al*. [21] grew rutile TiO_2 nanorod arrays on TiO_2 seed layer on fluorine-doped tin oxide (FTO) substrate by a hydrothermal method. The introduced TiO_2 seed layer was found to expressively increase the density and vertical alignment of the nanorod arrays, which led to the development of dye absorption and electron transport. By adjusting the $TiCl_4$ solution concentration, PCE of 2.55% could be achieved in a DSSC fabricated by TiO_2 nanorod arrays grown on seeded-FTO substrate using 0.15 M $TiCl_4$ solution, which was higher than the DSSC fabricated by nanorod arrays grown on bare FTO substrate (1.13%).

P. Zhong *et al.*[22] fabricated highly ordered TiO_2 nanotube arrays with the tube length in a very wide range between 10 and 100 μm, which were quickly fabricated on Ti sheets by using a modified electrochemical anodization process, and applied them to working electrodes of DSSCs having the back-illuminated device structure. The results specified that the as-prepared TiO_2 nanotube arrays had well-defined tube geometry, with a diameter around 100

nm and the nanotubes were in reality comprised by TiO_2 nanoparticles other than single crystals. A maximum power conversion efficiency of 4.25% could be achieved at an optimized nanotube length of 34 μm.

1.2.2 Nanowires (nanorods or nanotubes) fabricated by AAO template

Y. Li *et al.* [23] studied the synthesis of CdS nanowire arrays with a solution reaction method by injecting the reactants into the pores of the AAO membrane. After dissolving the AAO template in 1 M NaOH, the CdS nanowires were formed in AAO membranes with pore sizes of 48, 32 and 20 nm nanowire bunches were found. The diameters of the wires were almost the same as the pore sizes. This indicated that the AAO membrane could act as a good template for CdS nanowires, and the wires should be arrange into arrays.

K. Aisu *et al.* [16] synthesized well-defined TiO_2 nanorods or nanowires using the AAO-template method. Just by changing fabrication procedures, the nanorods and the nanowires were easyily fabricated. The abundance of TiO_2 nanorods with the length of 500 nm -1 μm and diameter around 200nm were investigated. The diameter of the nanorods was in good conformity with the hole diameter of the AAO template. The maximum length (60 μm) of nanowires was exactly in accord with the thickness of AAO template (60 μm). These results indicate that the length of 1-D nanostructured TiO_2 can be controlled only by changing the sample setting (whether IS or VDS) as shown in Fig. 1.1.

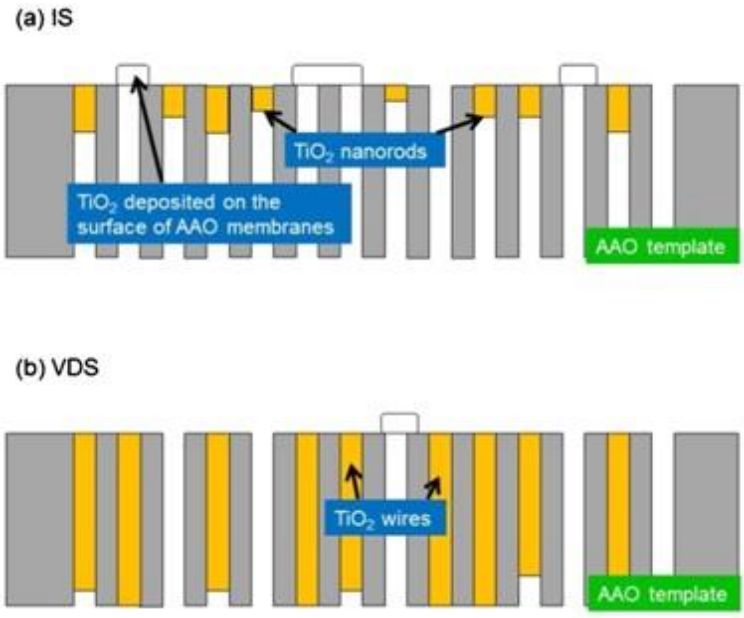

Fig. 1.1. Sample preparation: (a) immersion setting (nanorods) and (b) vacuum and drop setting (nanowires), and TiO_2 particles deposited on the surface [16].

K. Takahashi *et al.* [24] used a capillary-enforced template-based method to fabricate V_2O_5-TiO_2 composite nanorod arrays via filling mixtures of $VOSO_4$ and $TiOSO_4$ solutions into the pores of polycarbonate membranes, as shown in Fig. 1.2. For comparison purposes, pure V_2O_5 nanorod arrays were prepared through the similar template-based method with V_2O_5 sol and the sol was synthesized through the V_2O_5-H_2O_2 route. The nanorods completely covered a large area and projected out from the surface of ITO substrate. (The Li^+ intercalation capacity and applicable current density of V_2O_5-TiO_2 nanorods electrodes were higher than pure V_2O_5 at a molar ratio of V/Ti = 75/25, but lower for molar ratio V/Ti = 50/50.)

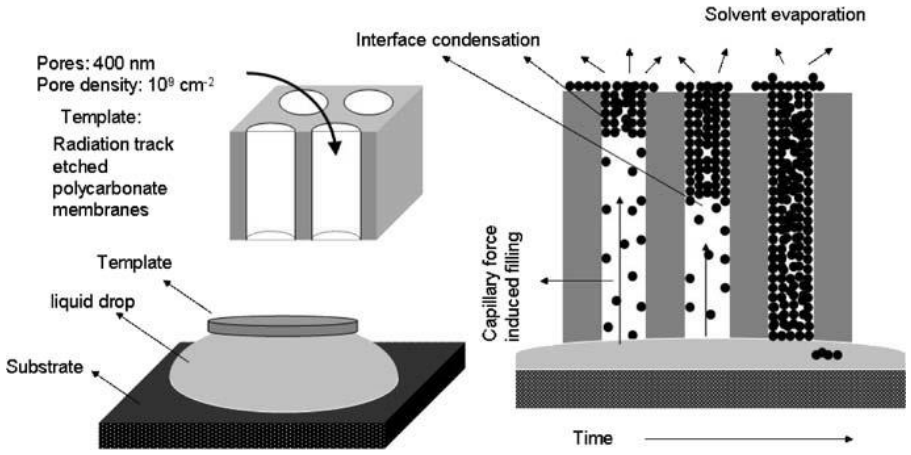

Fig. 1.2. Setting of a capillary-enforced template-based method to fabricate V_2O_5-TiO_2 composite nanorod arrays via filling mixture of $VOSO_4$ and $TiOSO_4$ solutions into the pores of polycarbonate membrane [24].

J. Lee *et al*. [25] fabricated nanotube arrays by atomic layer deposition with AAO templates and used in DSSCs as working electrodes as shown in Fig. 1.3. The obtained structures in the 2 types of nanotubes, closed-end and open-end, were produced by the reactive ion etching (RIE) process.

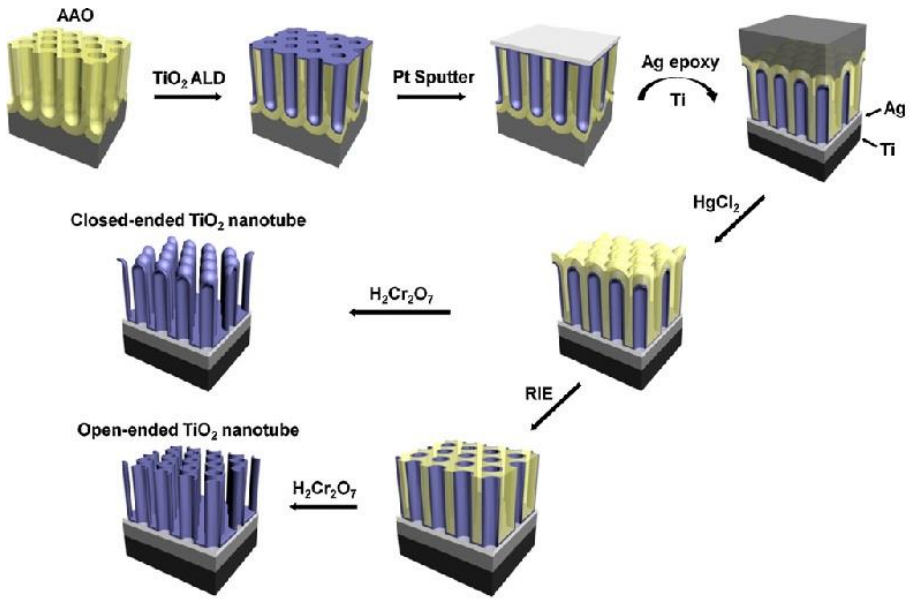

Fig. 1.3. Fabrication of DSSC working electrode using TiO_2 nanotube arrays with closed and open ends [J. Lee *et al*., 2012].

The DSSCs prepared from the TiO_2 nanotubes with open ends exhibited higher power conversion efficiency of 1.17% than those with closed ends.

T. Wen *et al.* [26] used the combination of sol–gel processing and centrifugation for the template-based growth of nanorod arrays. The centrifugation force drives the sol nanoclusters into the pores of the template, filling the pores to grow nanorods. The dense nanorods with diameters of around 200 nm and length around 10 μm were easily gained after heat treatment of polycarbonate membrane filled with polymeric SiO_2, colloidal SiO_2, TiO_2, and PZT sols.

S. Lee *et al.* [27] research template synthesis accompanied with hydrolysis by water vapor in the preparation of TiO_2 nanotubes (Fig. 1.4). These TiO_2 nanotubes were prepared within the pores of an AAO template. TiO_2 nanotubes diameters of ca. 50 and 200 nm were obtained by template synthesis. The nanotubes that had diameters at 50 nm were anatase polycrystalline structure. This difference between the template pore diameter and the TiO_2 nanotubes was because of the non-uniform pores of the commercial alumina membrane, which had a diameter of 20 nm at the top of the membrane and a diameter of 200 nm at the bottom of the membrane.

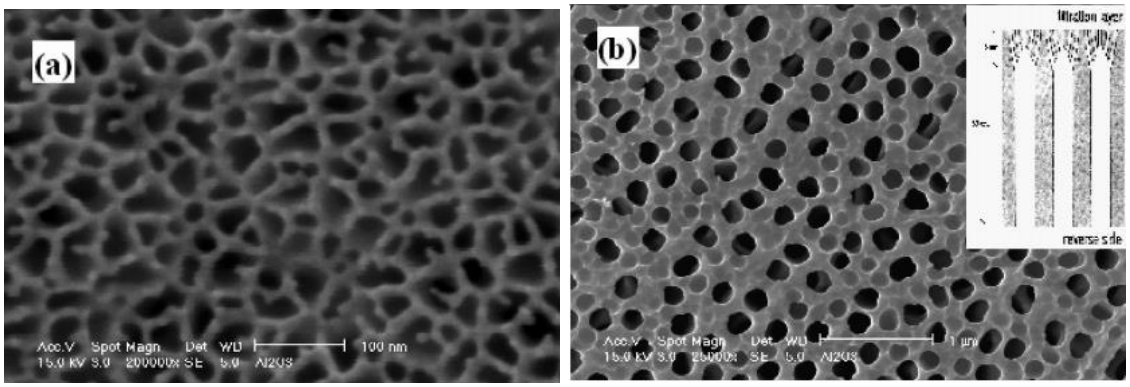

Fig. 1.4. SEM images of commercial Whatman anodisc (20 nm): (a) top view and (b) bottom view [27].

K. Aisu [16] reported on the fabrication of TiO_2 nanowires using the AAO template method. The template was removed by HCl treatment for 24-72 h. XRD patterns of the products showed disappeared broad peaks of AAO and the peaks of anatase TiO_2 (Fig. 1.5). These results indicated that AAO templates were successfully removed by the HCl treatment (>24 h).

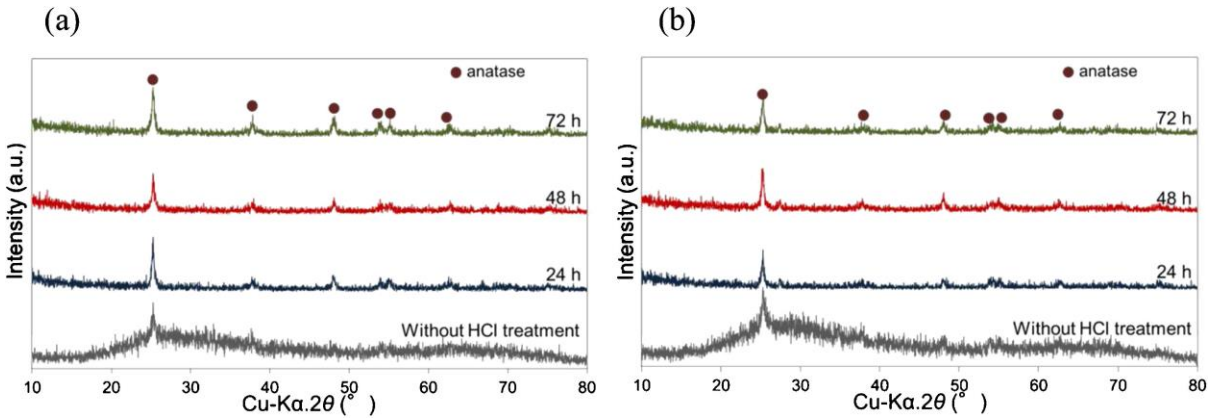

Fig. 1.5. XRD patterns of the samples without HCl treatment and with HCl treatment at 40°C for 24, 48 and 72 h: (a) immersion setting (IS), and (b) vacuum and drop setting (VDS) [16].

C.C. Tsai and H. Teng [28] demonstrated that nanotubes synthesized from a NaOH treatment on TiO_2 with subsequent acid washing could proceed with repeatable crystalline-structure transformation through a simple acid-base washing step (Fig. 1.6).

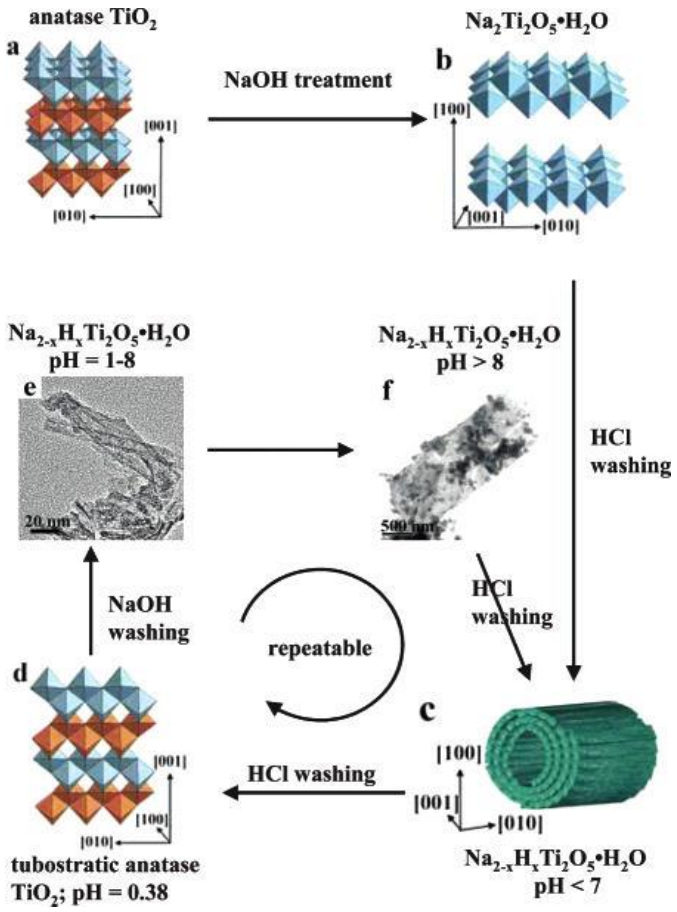

Fig. 1.6. Overall scheme for the formation and transformation of nanotube induced by the NaOH treatment and the post-treatment washing [28].

The solar cell parameters are summarized in Table 1.1 for different DSSCs made of semiconductor oxide nanostructured electrodes, which were fabricated from different fabrication methods fromliteratures. Table 1.2 compares photovoltaic characteristics (J_{sc}, V_{oc}, and *PCE*) of different DSSCs made of semiconductor oxide nanostructured electrodes which were fabricated from AAO-template combined with other fabrication methods mention in literature.

Table 1.1. Comparisons of photovoltaic characteristics (J_{sc}, V_{oc}, and *PCE*) of different DSSCs made of semiconductor oxide nanostructured electrodes which were fabricated using different fabrication methods.

Fabrication method	Diameter	Semiconductor Oxide	J_{sc} (mA/cm^2)	V_{oc} (V)	*FF*	*PCE* (%)	Ref.
Hydrothermal	10-70 nm	TiO_2 nanoparticles	12.1	0.74	0.63	5.59	[7]
		TiO_2 (10% nanowires+ nanoparticles)	13.2	0.74	0.66	6.53	[7]
		TiO_2 nanowires (100%)	5.1	0.71	0.71	4.13	[4]
		TiO_2 nanowires+ nanoparticles	8.2	0.74	0.64	2.42	[7]
	10-100 nm	TiO_2 (10% nanowires+ nanoparticles)	11.9	0.75	0.67	6.01	[4]
		ZnO nanowires+TiO_2	16.0	0.78	0.50	6.27	[14]
	≈200 nm	TiO_2 nanorod array	4.91	0.85	0.61	2.55	[21]
	1 μm	ZnO nanoparticles	2.60	0.76	0.57	1.13	[21]
	200 -250 nm	ZnO nanowire+ TiO_2 nanoparticles	8.04	0.67	0.40	2.15	[20]
	≈200 nm	Porous ZnO nanowire arrays	6.17	0.77	0.65	3.06	[29]

Table 1.1. Comparisons of photovoltaic characteristics (J_{sc}, V_{oc}, and *PCE*) of different DSSCs made of semiconductor oxide nanostructured electrodes which were fabricated using different fabrication methods. (Cont.)

Fabrication method	Diameter	Semiconductor Oxide	J_{sc} (mA/cm^2)	V_{oc} (V)	*FF*	*PCE* (%)	Ref.
One-pot NH_4OH hydrothermal	5-14 μm	TiO_2 nanotube arrays	6.17	0.59	0.49	4.25	[20]
Anodization	10-100 nm	TiO_2 nanotube arrays	9.51	0.71	0.56	3.58	[8]
	100 nm	TiO_2 nanotube arrays	8.99	0.59	0.49	4.25	[9]
	46-nm		7.87	0.75	0.49	2.9	[29]
			14.89	0.70	0.76	6.50	[30]
Solvothermal	4-6 nm	TiO_2 nanowire arrays	14.29	0.75	0.49	2.90	[31]

Table 1.2. Comparisons of photovoltaic characteristics (J_{sc}, V_{oc}, and *PCE*) of different DSSCs made of semiconductor oxide nanostructured electrodes which were fabricated from AAO-template combined with other fabrication methods.

AAO method	Diameter	Semiconductor oxide	J_{sc} (mA/cm^2)	V_{oc} (V)	*FF*	*PCE* (%)	Ref.
AAO+ solution	200 nm	TiO_2 nanorods	-	-	-	-	[16]
ALD+ AAO	70 nm	TiO_2 nanotube arrays	8.04	0.67	0.40	2.15	[25]
			2.6	0.72	0.58	1.10	[32]
		ZnO nanotubes	3.3	0.74	0.64	1.6	[33]
AAO+ solution	100 nm	TiO_2 nanorods	11.17	0.72	0.57	4.68	[32]

In this study, fabrication of TiO_2 nanowires (nanorods/semi-nanotubes) were fabricated using AAO templates. The size of the hole diameters of the templates and the fabrication settings (immersion setting (IS) and vacuum drop setting (VDS)) were focused. Obtained nanorods and semi-nanotubes were applied to photoelectrodes for DSSC applications.

1.3 Research Objectives

1.3.1 To synthesize 1-D TiO_2 nanorods/semi-nanotubes by AAO template method.

1.3.2 To characterize physical properties, electrical properties, and morphology of 1-D TiO_2 nanorods/semi-nanotubes

1.3.3 To combine nanoparticles and nanowires as semiconductors for application in DSSCs.

1.3.4 To improve the power conversion efficiency of DSSCs made of TiO_2 (in terms of photocurrent density, open circuit voltage and fill factor) as compared to those of the referent TiO_2 flat films.

1.4 Scopes of Research Work

1.4.1 This research focused on synthesized TiO_2 nanorods/semi-nanotubes using AAO templates with varied hole-diameter size (100 and 200 nm).

1.4.2 The setting to insert the precursor into the AAO pore were immersion setting (IS) (1-way open pore AAO template) and vacuum drop setting (VDS) (2-way open structure) at the same conditions.

1.4.3 Obtained nanorods and semi-nanotubes were applied to photoelectrodes for DSSCs. The efficiencies of the DSSCs made up of nanorods and semi-nanotubes were investigated and comparedto cells made of conventional flat TiO_2 films.

CHAPTER 2

THEORIES

2.1 Dye Sensitized Solar Cell (DSSC)

Nowadays, the current conventional solar cell is mainly based on the first generation of solar cells based on silicon. This type of solar cell challenged with electrical production from fossil fuels. However, the production cost still higher when compared with fossil fuel even China is now producing the crystalline silicon based solar cells and modules [9, 35-36]. The second generation solar cells, such as an amorphous silicon, CIGS, and CdTe, are based on thin film technologies. The advantages of thin film solar cells are including the ease of manufacture permitting a reduction of cost, various types of application and ability to use flexible substrates. However, the cost is only slightly lower than that of conventional silicon based solar cell mainly because of expensive manufacturing equipment and another problem is some rare earth material that difficult and dangerous for mining such as Cd or Te [9, 21].

In the challenge to achieve very low cost fabrication, the present attractive feature that make possible to industrial and separate entirely from the conventional solid-state junction device like first and second generation of solar cell, by replacing the contacting phase to the semiconductor by an electrolyte, liquid, gel or solid, thereby forming photo-electrochemical cell and devices based on networks of semiconductors, for example, nanofilm, nanoparticles, nanotubes, nanorods and nanowires. DSSC realizes the photon absorption and the charge separation processes by the relationship between a sensitizer as light-absorbing material and a wide band gap semiconductor of nanocrystalline morphology [16].

2.2 Device Structure and General Principle of DSSCs

A DSSC is comprised of a nanocrystalline structure semiconductor oxide, nanostructure electrode, dyes, electrolytes, counter electrode and transparent conducting substrate (glass). Normally, TiO_2 nanofilms/nanoparticles were used as photoanode but recently many combined nanostructures were also used as photoanodes. Pt/Au as counter electrode, filled with electrolyte solution of I_3^-/I^- in organic solvent, and then the sandwiched solar cells are produced [37-38]. The transparent semiconductor provides the pathway for electrons that

generated by photoexcitation to transport to the anode. The liquid electrolyte is the pathway from the cathode which provides electrons for oxidized dye.

Fig. 2.1. shows the production of the electrolyte reduced species at the cathode and the supply of electrons via the anode to the external circuit. The semiconductor network coated with dye molecules need to be transparent to allow light to reach the absorbing materials, and the network must have a massive surface area to provide the dye amount necessary for light absorption. The electrolyte must be able to fill the entire network to give electrical stability. Therefore, liquid electrolytes have been demonstrated to be very effective [9, 14, 16, 38].

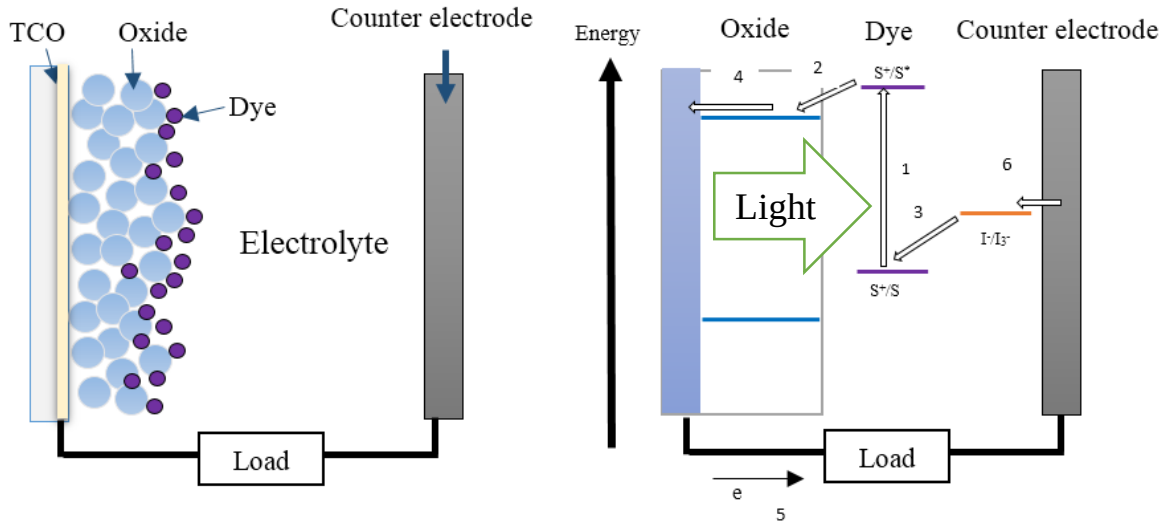

Fig. 2.1. Overview of a DSSC and basic electron transfer processes not including recombination process of simple energy diagram.

The general principles of a DSSC knowingly differ from a silicon solar cell. In silicon solar cells a *p-n* junction arise by combining p-type and n-type semiconductors with a very close contact and the processes of light absorption and charge transport occurin the same phase material. On the other hand, in DSSCs, these processes are occurred in different phase materials which evade the early recombination of electrons and holes. Consequences in DSSCs, high purity materials are not required as same as conventional silicon solar cells [35, 39].

2.3 DSSC Operation Principle

The operating principles of a DSSC can be described in this set of reaction equations [40]:

$$TiO_2/S + h\nu \rightarrow TiO_2/S^* \quad (2.1)$$

$$TiO_2/S + h\nu \rightarrow TiO_2/S^+ + e_{cb} \quad (2.2)$$

$$TiO_2/S^+ + e_{cb} \rightarrow TiO_2/S \quad (2.3)$$

$$TiO_2/S^+ + 3/2I^- \rightarrow TiO_2/S + 1/2\ I_3^- \quad (2.4)$$

$$1/2\ I_3^- + e_{Pt} \rightarrow 3/2I^- \quad (2.5)$$

$$I_3^- + 2e_{cb} \rightarrow 3\ I^- \quad (2.6)$$

The chemical reaction equations above show that the dye absorbs a photon and then an electron is excited from a low-energy state (highest occupied molecular orbital, HOMO) to a high-energy state (lowest unoccupied molecular orbital, LUMO) of the molecule *(2.1).* This is followed by electron injection to the TiO_2 conduction band *(2.2),* and the oxidized dye is regenerated by electron capture from the redox electrolyte *(2.3).* The injected electron travels by diffusion in the TiO_2 film and passes to the substrate contact where it is released to the external electrical circuit. The electron is returned to the cell via an electrolyte reduction reaction at the counter electrode *(2.4).* The electrical circuit of the cell is completed by ionic transport of the redox couples in the electrolyte *(2.5) and (2.6).*

Overall power conversion efficiency is not a lasting chemical conversion. Parallel to these processes, electrons in the conduction band of semiconductor may be recombined with the oxidized dye sensitizers or acceptor species in the electrolyte solution. This perhaps occurs by traps and intermediate reactions. The reaction is called "dark current", is the major loss function for the DSSC, as shown in the Fig. 2.2, indicate that further the preferred pathway of the electron transfer processes (processes 2, 3, 4, and 7) related to the chemical reaction equation above, the loss reactions 1, 5, and 6 are indicated. Reaction 1 is the direct recombination of the excited electron dye reflected by the excited state lifetime. Recombination of injected electrons in the TiO_2 with either oxidized dyes or acceptors in the electrolyte numbers as 5 and 6, respectively [36, 41-43].

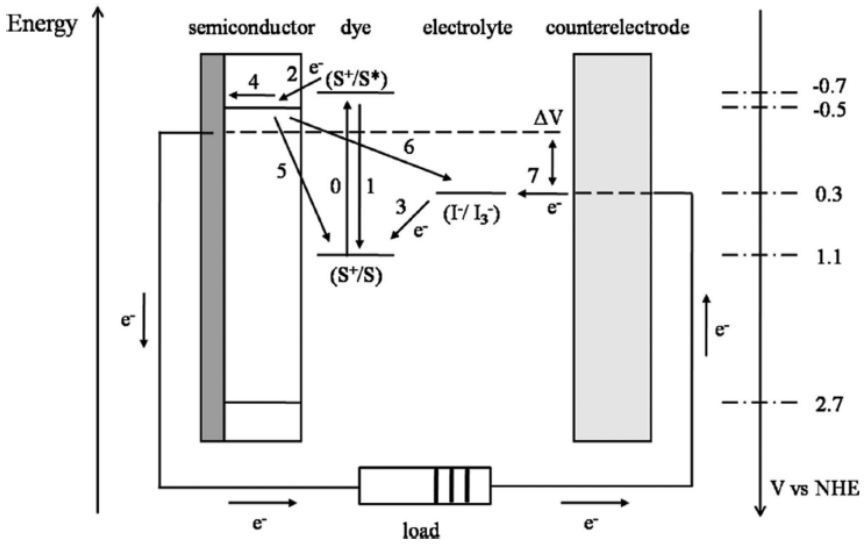

Fig. 2.2. Basic electron transfer processes are indicated by numbers (1-7) of simple energy level diagram for a DSSC [35].

2.4 Performance Characteristics

The figure of the I-V curve of a DSSC can be used with the simple diode equivalence circuit model in Fig. 2.3 [35, 38, 40] related to the following I-V equation:

$$J = J_{ph} - J_0[\exp(q\frac{V + JR_s}{nKT}) - 1] - \frac{V + JR_s}{R_{sh}}$$

(2.7)

where J and V are the output current density (A/cm^2) and voltage (V), respectively. J_{ph} is the photocurrent density (A/cm^2) as a current source, J_0 the reverse saturation current density (A/cm^2) of the diode, k is the Boltzmann constant (1.3806488 × 10^{-23} m^2 kg s^{-2} K^{-1}), q is the electron charge, T is the absolute cell temperature, n is the diode ideality factor, and R_S and R_{sh} are the specific series and shunt resistances (Ω/sq.) of the cell, respectively.

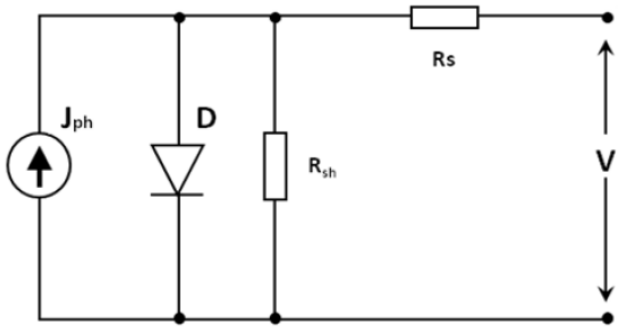

Fig. 2.3. Basic diode equivalent circuit model of a solar cell.

The diode model parameters can be determined by fitting the model to measure a solar cell I-V curve (Fig. 2.3). As shown in Fig. 2.4, J_{SC} is the short-circuit current density (A/cm^2); V_{OC} is the open-circuit voltage (V); FF is the fill factor. The fill factor is supposed to be values between 0 and less than 1 or the 'squareness' of the J–V curve and is explained by the ratio of the maximum power (P_{max}) of the solar cell per unit area divided by the V_{oc} and J_{sc} according to:

$$FF = \frac{Jm \cdot Vm}{Jsc \cdot Voc} = \frac{P_{\max}}{Jsc \cdot Voc} \qquad (2.8)$$

Assume that FF is equal to 1, a J-V curve influences the outer rectangular area. Numerous factors influence FF, such as high inner resistance, which from a bad counter electrode, decreases FF and overall efficiency. The overall light-to-electrical energy conversion efficiency, also called the power conversion efficiency (PCE), is given by the multiplied values between J_{sc}, V_{oc} and FF divided by P_{in}.

$$PCE = \frac{Jsc \cdot Voc \cdot FF}{Pin} \qquad (2.9)$$

Standard intensity input power is 1000 W/m^2 (100 mW/cm^2). Therefore, there are 3 major characteristics that determine the efficiency of the device (J_{sc}, V_{oc}, and FF).

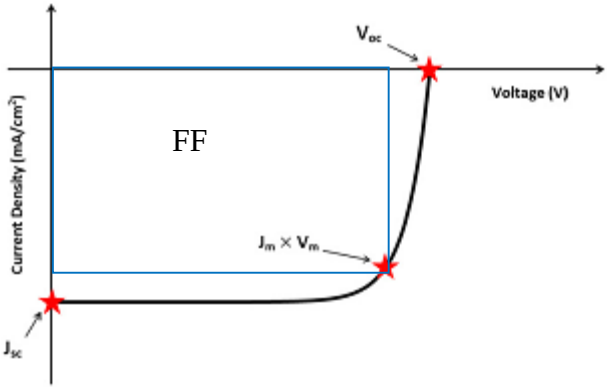

Fig. 2.4. Current density–voltage (J–V) characteristics for a generic illuminated solar cell, indicates the 3 major device characteristics that determine PCE [modified from 40, 35].

2.5. Materials in DSSC

2.5.1 Transparent conducting oxides (TCOs)

DSSC devices require 2 electrodes at the front and rear sides of the device to provide both optical access and a low-resistance electrical connection. For DSSC applications, the choice of TCO is determined by additional considerations, including work function, band alignment, materials compatibility, processing, and cost. Normally, fluorine doped tin oxide ($F:SnO_2$ or ITO) is used as the back contact for the nanostructured TiO_2 (anatase). The transferring of holes to the TCO front electrode is helped by Pt particles at counter electrode that accelerated the electron transfer. Table.2.1 is an overview about types of TCOs those used in present solar cells [39, 37].

Table 2.1. TCOs employed in photovoltaic devices [41].

Cell type	TCO in current use	TCO needs	Materials goals
Heterojunction with intrinsic thin layer	Indium tin oxide (ITO)	Smooth, good interfacial properties very good conductivity, Low temperature deposition, light trapping	Indium zinc oxide (IZO), indium-free ma terials, ZnO
Copper indium gallium selenide (CIGS)	Intrinsic-ZnO/Al:ZnO	Interfacial stability to CdS, low-temperature deposition, resistance to diffusion and shorting, need to make/improve the junction	Single-layer TCO to replace 2 layers and CdS layer
CdTe	(SnO_2) Zn_2SnO_4/Cd_2SnO_4	Stable interface to CdS/CdTe at temperature, diffusion barrier	Doping of ZnSnOx materials, single-layer TCO

Cell type	TCO in current use	TCO needs	Materials goals
Hybrid polymer cell	ZnO, SnO_2, TiO_2	Nanostructure with right length scale, work-function matching, interface with organic, correct doping level for carrier transport	Self-organized structures core–shell structures, new nonconventional TCOs
DSSC	TiO_2, ITO, FTO	Nanostructure with high electron mobility	Improved TiO_2 morphology and possible use of doped materials, new non-TiO_2 materials
Amorphous Si	SnO_2, ITO, and ZnO; many cells employ 2 TCOs	Temperature stability, chemical stability, and appropriate texture for both TCO layers	Higher conductivity texture, and ohmic contact for both TCO layers

2.5.2 Oxide semiconductors

Nanostructured materials present a notably larger surface area than that of bulk materials. The nanoscale size may also affect the behavior of electrons transporting in nanostructures in view of a limit to the electron mean free path. Semiconductor oxides such as TiO_2, ZnO and SnO_2, have been under extensive study because of their broad applications in energy and environmentally friendly materials. These materials work as an electron transfer pathway because of their conductive electronic structure, referred to valence band (VB) and conduction band (CB). Band positions of several generally used semiconductors are shown in Fig. 2.5.

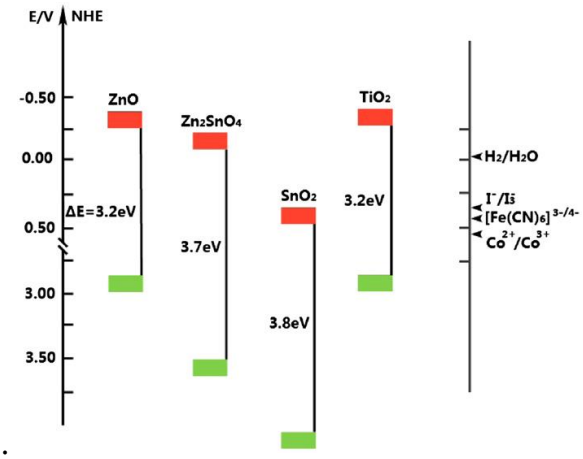

Fig. 2.5. Band positions of several semiconductors and potentials of redox electrolyte [36].

In quantum physics theory, a photon with an energy that exceeds or matches the band gap (E_g) of a semiconductor can excite an electron to the conduction band, leaving a hole with a positive charge at the valence band. These charges can either be transferred to the external circuit to provide electrical current or be utilized to catalyze a certain chemical reaction [16, 37, 39, 42].

2.5.3 DSSC Dyes

The dye in DSSCs absorbs the photon and creates an electron. It allows the electron to be injected into the conduction band of the semiconductor. There are 2 classes of dyes: organometallic and organic dyes. Organometallic dyes contain a transition metal in the structure while organic dyes can be indoline-derived dyes, porphyrin-based complexes, benzothiazolemerocyanine based dyes, oligoene dyes, and coumarin derivatives. Currently, the most efficient DSSCs are ruthenium-based sensitizers, such as N3, N719, Z907 and black dye [9, 16, 21, 37, 36]. A dye is adsorbed on the semiconductor surface generally by special anchoring groups connected to the dye molecule. In the organometallic dye these are the carboxylic groups (COOH) at the end of the pyridyl rings. The COOH groups bonded with the TiO_2 surface by donating a proton to the TiO_2 lattice [35, 40, 41]. Fig. 2.6 shows some molecular structures of 3 efficient photosensitizers for DSSCs including N3 dye, black dye, and N719.

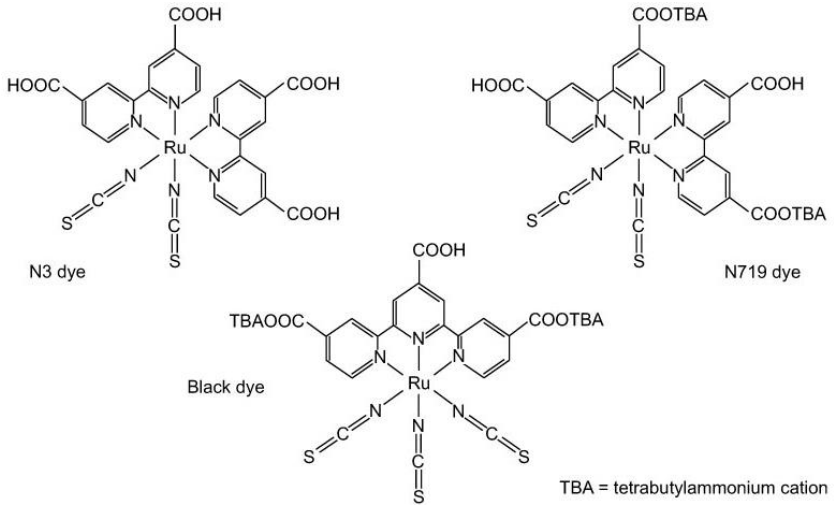

Fig. 2.6. Molecular structures of 3 efficient dyes for DSSC [modified from 35, 40].

2.5.4 Iodine based electrolytes

Iodide/triiodide couple has good solubility, does not absorb too much light, has a suitable redox potential, and provides rapid dye regeneration. However, the isolation of I^-/I_3^- from most redox electrolytes is the very slow recombination kinetics between the electrons in TiO_2 and the oxidized part of the redox couple, triiodide. Certain dyes adsorbed at TiO_2 catalyze this recombination reaction, presumably by binding iodine or triiodide [42, 43].

Iodine based electrolytes can be optimized in terms of efficiency and stability. Increased efficiency is usually achieved by varying the solvent, adding coadsorbents or changing the counterions of iodide. The optimization process is unique for each dye/electrolyte combination. A better stability can be obtained by modifying the TiO_2-dye interface or reducing the vapor pressure of the electrolyte solvent.

2.5.5 Counter electrodes

Conventionally, platinum (Pt) or gold (Au) catalyst was deposited on a transparent conductive oxide substrate is used as a counter-electrode in DSSCs. The counter electrode is used as a cathode, which plays a role for the I_3^- reduction and electron transfer. The performance of the counter electrode needs the low internal resistance and raw material cost. Until now, the best performance material for the counter electrode is Pt, which exhibits excellent electrochemical activity of the I_3^-reduction at film thickness of 2-10 nm. In an aim to obtain the preferred catalytic performance for the I_3^- reduction, the appropriate amount of Pt is around 5-10 mg/cm^2 [44, 45].

2.5.6 TiO_2 as Anode Materials

TiO_2 is a stable, nontoxic oxide, which has a high refractive index (n ≈2.4-2.5) and is widely used as a white pigment for painting, sunscreen, self-cleaning materials, and food. Various crystal forms of TiO_2 occur in nature: rutile, anatase, and brookite, as shown in Fig. 2.7 [16, 7, 25, 38].

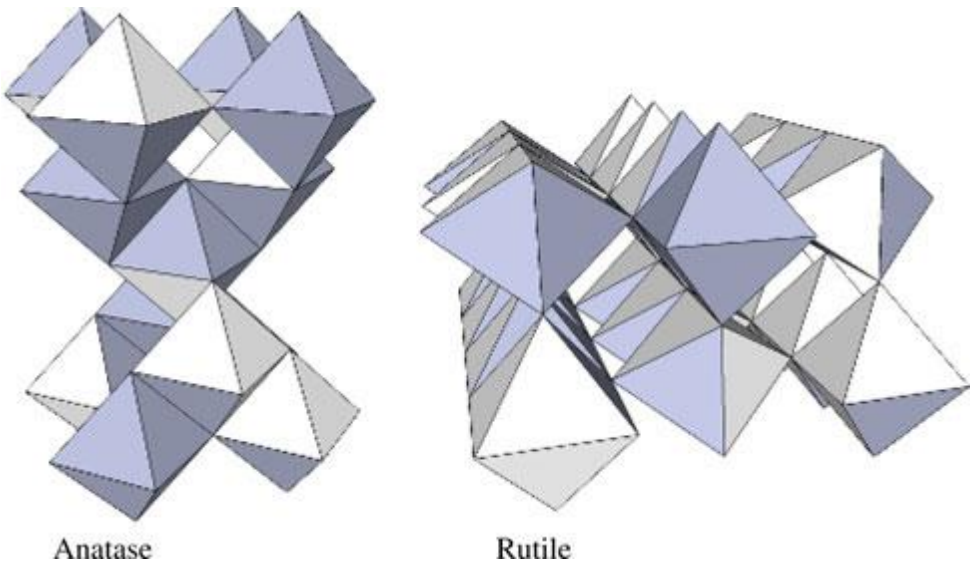

Fig. 2.7. The TiO_2 group is composed of rutile and anatase [46].

Rutile is the most stable form in thermodynamic terms. Anatase is, however, the favored structure in DSSCs, because it has a wider bandgap (≈3.2 compared with 3.0 eV for rutile) and higher conduction band edge energy. This leads to a higher Fermi level and V_{oc} in DSSCs for the same conduction band electron concentration. The improvements to the TiO_2 electrode in the DSSC have been made in terms of light absorption, light scattering, charge transport, suppression of charge recombination, and improvement of the interfacial energey. Charge transportation depends on nanostructured semiconductor oxide. Amongst different nanostructures, nanoparticles have been most widely studied for use in DSSCs to form photoelectrode film. Starting with nanoparticles properties, nanocrystalline semiconductor TiO_2 particles are of interest due to their high specific area for dye and several potential technological applications, such as photocatalysis, sensors, solar cells, and memory devices [35].

However, the presence of several boundaries in the nanocrystalline particles has been estimated as an unfavorable reason that may increase interfacial charge recombination happened between the photogenerated electrons and the positive species in the electrolyte. Fig.

2.8 shows the possible origins of the relatively slow diffusion. Traps can be located at the TiO_2/electrolyte interface, in the bulk of the TiO_2 particles, or at grain boundaries, whereas electro\static interactions between electrons and ions in the electrolyte cause ambipolar diffusion but possibly also trapping [40].

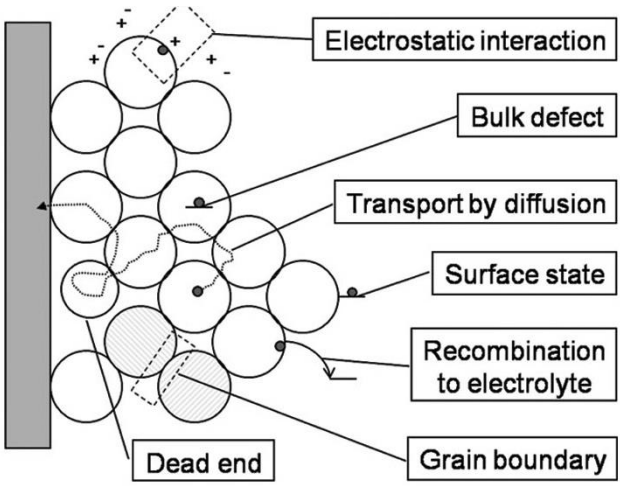

Fig. 2.8. The electron transport process in the electrolyte-infiltrated mesoporous TiO_2 electrode of a DSSC [9].

Inferior in terms of PCE to those cells using conventional nanoparticles, because of their slow electron percolation through the interconnected nanoparticles, poor charge transfer to TCO and the random contact between the disordered TiO_2 nanoparticles acts as a grain boundary leading to trap and recombine of electrons, which limits the efficiency of the DSSCs. To improve charge transfer, negative electrodes comprised of well-ordered and strongly interconnected 1-D nanomaterials, such as nanorods or nanotubes, have been proposed [4, 8, 16, 20]. One-dimensional nanomaterials are estimated to transport electron faster than nanocrystalline films. These have been proved by many experiments which reveal that the electron transport in photoelectrode comprised of single crystal nanowires and nanotubes are faster than that in the case of nanocrystalline film [4].

A fast electron transport may lower the opportunity of photo-generated electrons to react with the positive species in the electrolyte, therefore, significantly suppress the interfacial charge recombination. However, the TiO_2 nanotube is interesting due to its high surface area, its thermal stability is poor and it easily fragments into nanoparticles at a temperature of around 500-600 ◦C, which is close to the sintering temperature of the DSSC electrode [9, 14, 21].

With the aim to prepare efficient electron transfer pathways comprised of well-ordered and strongly interconnected 1-D nanomaterials, such as nanorods or nanotube arrays, have been proposed using 1-D TiO_2 nanomaterials is a straightforward way to realize the "electron expressway concept" as shown in Fig. 2.9.

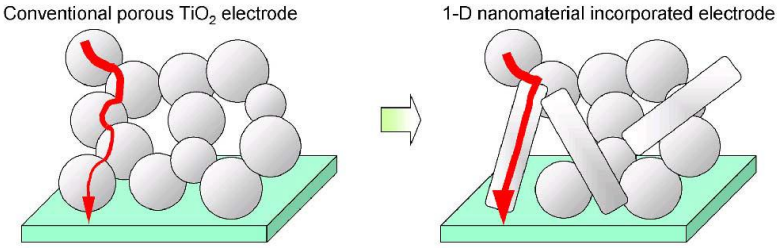

Fig. 2.9. "Electron expressway concept" shows movement in convention metal oxide nanoparticles and metal oxide (up) nanowire mix with nanoparticles and (down) only ordered nanostructure [4].

The nanowire-structured TiO_2 therefore forms a promising alternative candidate to the nanotube for a DSSC electrode. Solid TiO_2 nanowires can be synthesized by a hydrothermal process at temperatures typically between 150-170 ◦C followed by the appropriate calcination process. These are expected to show better thermal stability. The comparison advantages and disadvantages of 3 TiO_2 nanostructures are shown in Table 2.2.

Table 2.2. Comparisons of various TiO_2 nanostructures for DSSC applications.

Morphologies	Properties	Disadvantages
Nanoparticles	High specific surface area	Growth condition more restricted, interfacial charge recombination, Traps.
Nanowires, nanorods	Less recombination because of the high-order for charge transfer, fast electron transport, good chemical stability in addition to high electron mobility.	Small surface area than nanoparticle and nanotube
Nanotubes	Less recombination because of the high-ordered for charge transfer**,** fast electron transport**,**	Thermal stability is generally poor and it easily fragments into

	surface area larger than that of nanowires or nanorods	nanoparticles at sintering temperature in DSSC application

At this time, numerous companies has been developed the methods to synthesize anatase nanostructured for example nanoparticles, nanorods, nanowires, nanobowls, nanosheets, and nanotubes and mesoporous materials. These methods comprise of sol-gel,hydrothermal, solvothermal, sonochemical, microwave deposition technique, direct oxidation, chemical vapor deposition, physical vapor deposition, and electrodeposition [9, 16, 21].

2.6 TiO_2 Nanowire Fabrications via AAO Template Method

TiO_2 is broadly used for many applications. Leaning on the various applications, various methods have been reported to synthesize 1-D TiO_2 nanomaterials. Among others, 3 methods are normally used, viz., (1) hydrothermal method, (2) anodic oxidation method, and (3) AAO template method. Hydrothermal method is relatively mass-productive. However, the size control, in particular for the length of 1-D structure, is not so precise. Anodic oxidation method is a synthesis process that gives TiO_2 membranes with well-ordered pores by from this method; however, it is difficult to separate each nanotube from membranes and limited for a certain metals. AAO template method is a synthesis process that AAO film with uniform pores is used as a template for 1-D nanostructure. A template synthesis has recently proved to be an elegant, inexpensive, inexpensive, and technologically simple approach. Generally, chemical solution processes are combined to this process to obtain uniform 1-D nanomaterials. By using this method, well-controlled separate 1-D TiO_2 nanomaterials can be obtained [17].

2.6.1 Basic properties of AAO

The structure of AAO was described as a closed-pack hexagonal array with cylindrical shapes of the nanopores as shown in Fig. 2.10. There are many parameters to be concerned when determined pore structure, for example, pore organizing (hexagonal shape), pore diameter, pore length, wall thickness, inter-pore distance, and barrier layer. These parameters can be controlled by controlling anodization condition. Anodization condition that can be tuned of Al metal such as; applied voltage, current, pH and electrolyte type, composition and concentration, and temperature or pre-patterning on the surface.

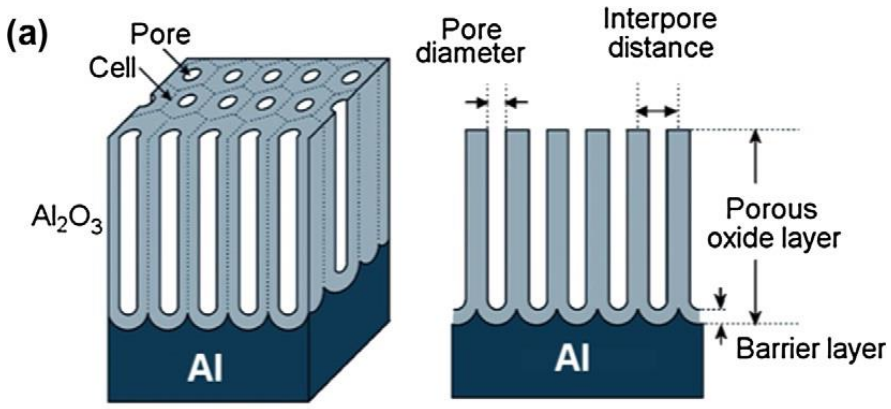

Fig. 2.10. Drawing of AAO structure prepared by electrochemical anodization of Al [modified from47]

AAO with desired and tunable pore structures can be achieved by using 3 well-known electrolytes, including sulfuric acid (H_2SO_4), oxalic acid ($H_2C_2O_4$), and phosphoric acid (H_3PO_4). With these kind under conventional anodization conditions, called "mild" anodization (MA), ordered arrays of AAO nanopores can be obtained. In a 2-step anodization approach, the first step is removal of the first generated porous layer, lead to pre-structure of Al and use this structure for long range order over the entire surface [17].

2.6.1 Theory of AAO template

The mechanisms for growth of AAO films in the early stage, the most researchers agreed that diffusion of cation and anion in the solution is possible through the dense oxide layer. Under the applied electric field, anion move to the oxide-metal interface and cation move toward solution-oxide interface. This 2-ways diffusion let the porous AAO layer grow thicker [47, 17], as shown in Fig. 2.11. There are 3 electrochemical reactions could be occurred at the metal-oxide interface; (1) oxidation of Al metal, (2) reduction of proton, and (3) oxidation of oxygen ion.

Solution-Oxide surface

$$Al^{3+} + 3O^{2-} \quad Al_2O_3$$

$$Al_2O_3 + 6H^+ \rightarrow 2Al^{3+} + 3H_2O$$

Metal-Oxide interface

$$Al \rightarrow Al^{3+} + 3e$$

$$2H^+ + 2e \rightarrow H_2$$

$$2O_2^- \rightarrow O_2 + 4e$$

$$2Al^{3+} + 3O^{2-} \rightarrow Al_2O_3$$

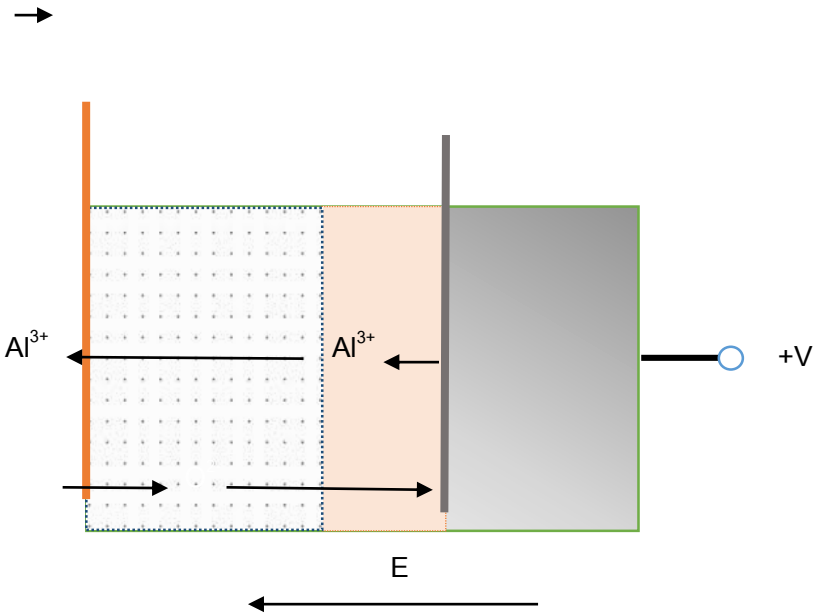

Fig. 2.11. Fundamental growth of AAO in acidic solution. O^{2+} represents any cations in the solution that could be combined with Al^{3+} to form Al_2O_3.

The electrochemical reactions at the metal-oxide surface resulted in the etching of aluminum and bubbling of H_2 gas. As long as anions (O^{2-}) arrived at metal-oxide interface, they were neutralized by oxidized (Al^{3+}) to form insoluble Al_2O_3. For clearly understanding, self-ordering electrochemistry for nanopore formation during anodization is reported [48] for metal and their alloys including Al, Ti, Ta, Hf etc.

Nanowires, nanorods or nanotubes can be prepared by electrodeposition or solution technique filled into the nanopores followed by the removal of the AAO template. The AAO structure can be described as a close-packed hexagonal array of parallel cylindrical nanopores perpendicular to the surface on top of the underlying Al substrates (Fig. 2.12.). By controlling anodization conditions, these parameters can be exactly tuned in the range of about 10–400 nm for pore diameter, 50–600 nm for interpore distance, pore aspect ratio from 10 to 5000 and a thickness of the porous layer from 10 nm to 150 lm [42].

This AAO method would be compose of the complex processes together with careful preparation of the template, electrode incorporation for the electrodeposition, removal of the barrier layer, suitable electrolyte selection, and the final template removal step. However, the nanotubes' diameter distribution can be well controlled in accordance with the template, the nanotubes' composition can be tuned in a wide range depending on the precursors in different

steps of the electrodeposition, and also the orientation can be controllable by adjusting the potential in certain cases [48]. Although, it is difficult to separate each nanotube from membranes. By using this method, well-controlled separate 1-D TiO_2 nanomaterials can be obtained in Fig. 2.12.

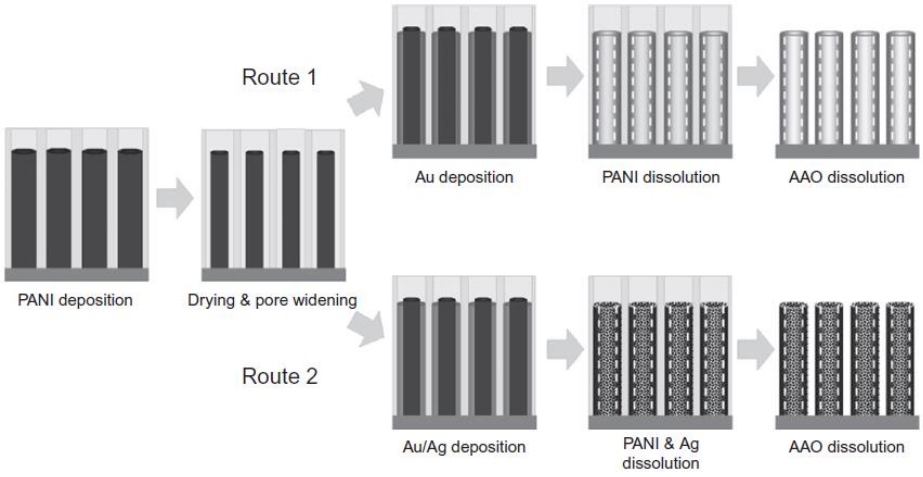

Fig. 2.12. Smooth and porous Au nanotube into the AAO template via electrodeposition [49].

There are many advantages of AAO, such as easy to fabricate structures with controlled structural properties, uniformity of pore diameters giveing uniform nanostructured geometry with high aspect ratios, and easy dissolution of AAO template with acidic or alkaline solutions without affecting the fabricated nanostructures confined inside the nanopores [45,48]. A 60-µm-thick nanoporous AAO template fabricated by the one-step anodization method is commercially available, for instance, from Whatman (Anopore® or Anodisc®) with 3 nominal pores size of 20, 100 and 200 nm and in 3 diameters: 13 mm (Anodisc13), 25 mm (Anodisc25) and 47 mm (Anodisc47). A significant drawback of those commercial templates is lack of order in the nanopore arrangement and nonuniform of declared pore diameter [17].

CHAPTER 3
METHODOLOGY

3.1 Preparation of TiO_2 Nanowires from AAO Templates

3.1.1 Materials used

$C_{12}H_{28}O_4Ti$ (tetraisopropyl orthotitanate, TTIP, TCI Ltd., Lot no. T88NH) was used as a Ti precursor, $(CH_3)_2CHOH$ (isopropanol, i-PrOH, TCI Ltd., Lot no. ELB6A) as a solvent , $C_5H_8O_2$ (acetylacetone: ACA, TCI Ltd., Lot.) was used as a chelating agent [27]. The ACA was added for helping to slow down the hydrolysis reaction of TTIP. The composition ratios of TTIP:ACA equaled to 1:1 (in molar ratio) and after that a ratio of TTIP:(ACA + i-PrOH) equaled to 1:4 (in volume ratio) [16]. TiO_2-precursor solution was prepared as follows. ACA was dropwisely added to TTIP, leading to a yellowish solution. After that, i-PrOH was dropped to the TTIP-ACA solution and then the color of the solution turned into transparent light yellow.

3.1.2 Immersion setting (IS)

AAO membranes (Whatman, Anodisc 25 and Anodisc 13) were used as the templates for 1-D TiO_2 nanomaterials. The AAO had the through-hole diameters of 100 nm and 200 nm. For immersion setting (IS), the AAO template was immersed into the TiO_2 precursor solution for 1 min under slightly decompressed atmosphere, as shown in Fig. 3.1 (a).

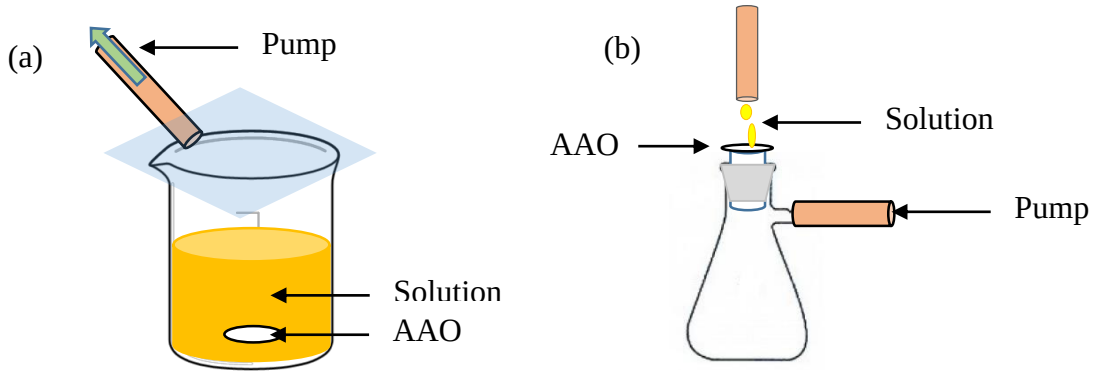

Fig. 3.1. Schematic illustrations of AAO-template methods: (a) immersion setting (IS) and (b) vacuum and drop setting (VDS).

3.1.3 Vacuum drop setting (VDS)

For vacuum and drop setting (VDS), the AAO template was put on the filtering flask as a cover plate, as shown in Fig. 3.1 (b). The precursor solution was dropped on the AAO template for 5 min with vacuuming from the bottom side of the AAO template. After that heating and the calcination of template were carried out as same as IS experimental procedures.

After inserting precursor solution, AAO membranes were left in the air around 30 min to progress the hydrolysis reaction in the precursor solution. By hydrolysis, color of AAO membranes was changed into whitish due to the deposition of TiO_2. Then, the samples were calcined at 450°C (for anatase phase TiO_2) for 1 h in air.

3.1.4 Template dissolution

After calcinations, samples were washed by 1 M hydrochloric acid (HCl, Wako Ltd, Lot. WER5708) to remove AAO templates from the samples. The samples after calcinations were put in a centrifuge tube filled with 1 M HCl. Then, they were mildly treated at low temperatures at 40°C for 24 h, 48 h or 72 h. After the HCl treatment process, the samples were separated into solid phase (TiO_2) and a liquid phase by centrifuging at 10,000 rpm. This step was same with AAO dissolution by 1 M NaOH solution.

3.2 Characterizations of 1-D TiO_2 Nanorods or Semi-nanotubes and AAO Template

The microstructure of nanoparticles, nanorods, nanowires and AAO template were characterized by scanning electron microscopy (SEM, JEOL) and field emission scanning electron microscopy (FE-SEM SU-70, HITACHI, Osaka Univ., V_{acc} = 5.0 kV). The crystalline structure was investigated by an X-ray diffractometer (XRD, 40kV, 40 mA, Multiflex KYD007-016, Rigaku, Japan). To clearly understand a procedure in this research, Fig. 3.2 shows a flow chart of each process, i.e., synthesis of nanorods or nanowires, fabrication of DSSCs made of synthesized nanorods or nanowires, and characterizations.

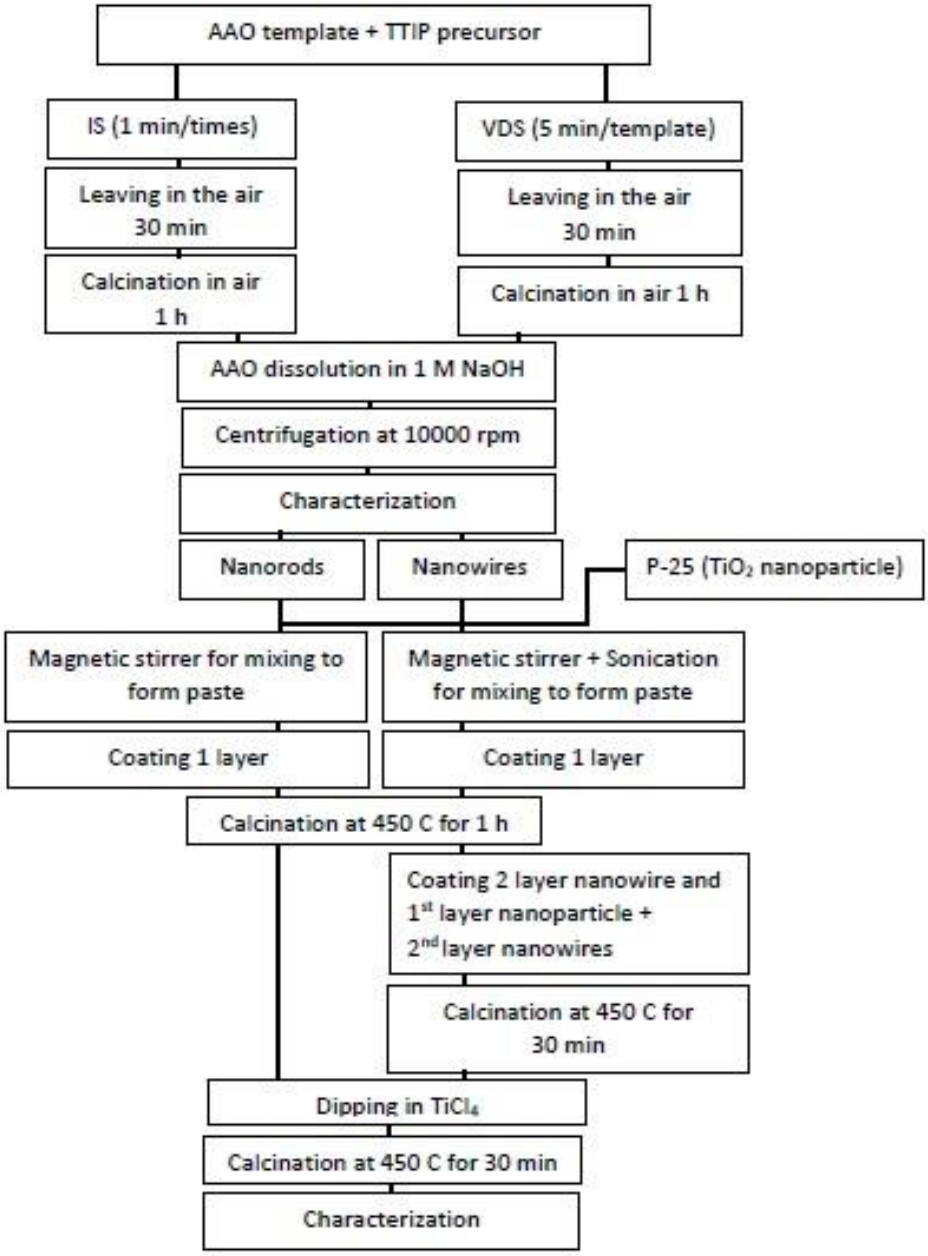

Fig. 3.2 The flow chart shows the procedure in each process, i.e. synthesis of nanorods or nanowires, and fabrication of DSSCs made of synthesized nanorods or nanowires and characterizations.

3.3 Fabrication of DSSCs

3.3.1 Conventional DSSC fabrication

TiO_2 paste preparation

Indium doped tin oxide (ITO) glass (Type 0052, 10Ω/sq., Geomate Co.Ltd., Yokohama, Japan) was used as TCO in this work. High thermal-resistant ITO glass, which can stand at the

high sintering temperature of DSSC at 450ºC without increasing of internal resistance and still can maintain high conductive properties. It was cut in a size of 3x1 cm^2 by a glass cutter (CAMAG, smartCUT). Then, it was washed by ethanol and put in an ultrasonic bath for cleaning for about 5 min. A TiO_2 nanoparticle paste was prepared by mixing 0.3733 g of TiO_2 nanopowder (P25, Nippon Aerosil Co., Ltd.) and 0.1750 g of polyethylene glycol (MW: 20,000, $(H(OCH_2CH_2)_nOH$, PEG, Lot. WEJ6692 Wako Pure Chemical Ltd., Tokyo, Japan) (as an organic binder) in 1 ml of distilled water. A drop of acetylacetone ($C_5H_8O_2$, ACA, 99.9%, Wako Pure Chemical, Lot No.TLN0469) was added to the paste to prevent aggregation of TiO_2 particles. All materials were pestled together in a porcelain mortar for 20 min. The paste was then coated on a clean ITO glass using the squeegee technique with an electrode area of 1 cm^2. After coating of TiO_2 on ITO glass, the cell samples were put on a hot plate (ECONOMY HOT PLATE, EHP-170N) to heat at 100 ºC for evaporating some water content and volatile materials from the cell surface. After the heating process, the obtained photoelectrodes were put on a heat-resistant dish and were then sintered in an electric furnace at 450 ºC for 30 min. The condition in this research for all samples was kept uniform as much as possible.

Dye adsorption on TiO_2 photoelectrodes

A solution of ruthenium (II) dye (N719, 0.3 mM) [Di-tetrabutylammonium cis-bis(isothiocyanato) bis(2,2'-bipyridyl-4,4'-dicarboxylato) ruthenium (II) 95% (NMR), molecular weight: 1188.55 (Aldrich, Lot. MKBN7892V)] was dissolved in 20 mL of ethanol (CH_3CH_2OH) then mixed by ultrasonic stirring (As One) for 5 min. Before soaking the cell in the dye solution, it was wiped using tissue with ethanol only on the glass surface for dust cleaning. Adsorption of dye on TiO_2 photoelectrodes was carried out by soaking the cells in the dye solution. The dye adsorption box was wrapped by a film and an aluminum foil for prevention of solution evaporation and degradation of dye by light, respectively. The dye adsorption box was then kept in an oven at 40 ºC for 24 hours.

Preparation of Pt counter electrode

Platinum (Pt) was deposited on the ITO glass as a counter-electrode by sputtering by a Pt coater (JEOL, JFC-1600 auto fine coater, University of Tsukuba). The current used was 30 mA and the time of sputtering was 60 s. Afterwards, the thickness of Pt film coated on ITO glass was achieved at 30 nm.

*Synthesis of **e**lectrolyte*

The electrolyte used in this research was a mixed solution of 0.1 M LiI (Wako, Lot. WEF3819, MW: 133.85) solution, 0.05 M I_2 (99.9%, MW_I = 126.904, Lot. WEP0909, Wako

Pure Chemical) solution, 0.6 M PMPII (1, 2-dimethyl-3-propylimidazolium iodide [$C_8H_{15}IN_2$, purity>98.0%, MW=266.13, Lot. SLDYF-AB, TCL] solution, and 0.5 M TBP (4-tert-butylpyridine, $C_9H_{13}N$, 96%, MW= 135.21, d (25 ºC) = 0.923 g/ml, Lot. SHBD4842V, Wako Pure Chemical) solution, in 1.25 ml acetronitrile (CH_3CN= 41.05, 99.5%, d= 0.780-0.784g/ml, Wako Pure Chemical, Lot. AWM0857). The mixed solution was stirred for 5 min in an ultrasonic stirrer for the homogenous electrolyte solution.

3.3.2 Modified fabrication for improvement of DSSC performance

The conventional/previous procedure was improved to increase the efficiency of DSSCs. TiO_2 paste, treatment of TiO_2 by $TiCl_4$ solution, and higher dye adsorption were modified.

Paste preparation for improvement of DSSC performance

Nanoparticle paste was prepared by the mixing of P25 TiO_2 powder (0.375 g), PEG (0.1 g), distilled water (0.4 ml), and ethanol (0.3 ml) and acetone (2,4-Pentanedione, $CH_3COCH_2COCH_3$= 100.12, 99.0% solubility in water and ethanol, d (20 ºC) = 0.971-0.976 g/ml) (0.04 and 0.08 ml). It should be noted that, in the mixing of PEG, PEG was dissolved in water first because PEG did not dissolve in alcohol. A magnetic stirrer (ASONE, magnetic stirrer REXIM RS44-R) was used to help for homogenous mixing. Initially the water with PEG was stirred at a low speed of 250 rpm and the speed was then increased to 600 rpm to continue stirring for several minutes until ~~all~~ PEG was perfectly dissolved in water. Afterwards, ethanol and acetone (0.04 ml) were added. P25 TiO_2 powder was then added into the mixed solution with simultaneously increasing speed until 600 rpm. The stirring was kept continued at the same speed for 20 min. Subsequently, the mixed solution was further stirred with additional acetone (0.08 ml) for 10 min. The paste was then achieved. The paste coating technique and steps were same as those used for the conventional DSSCs. Finally, the cell was dried on heater at 80-100 ºC for evaporation of some water content and then put in an electric furnace for sintering at 450 ºC, 1 hr.

$TiCl_4$ treatment for improvement of DSSC performance

An 80 mM $TiCl_4$ (0.0065 ml) solution was prepared with distilled water (7.5 ml) at 1 ºC to prevent the precipitation of TiO_2 due to the highly exothermic hydrolysis reaction. If the temperature of water reaches room temperature, the reaction will start quickly and the solution will turn into whitish. The DSSC photoanodes were dipped into the solution perpendicularly to the bottom of the container. The height of the solution should be concerned, because if it is too high, TiO_2 particles can deposit away from the desired area. After dipping of photoanodes

in a solution for 30 min, the photoanodes were taken out and dipped in ethanol for rinse. Lastly, the photoanodes was dried at 80 ºC on a heater to evaporate water and then sintered again at 450 ºC for 30 min.

Dye adsorption for improvement of DSSC performance

For improvement of DSSC performance, a 0.5 mM solution of N719 was used instead of 0.3 mM one. A given color of this dye was darker than the dye by the previous procedure. Other steps for dye preparation were the same as those by the conventional processes.

3.3.3 DSSC assembly

For both conventional and modified preparation, all DSSCs had an opened cell structure. A 100 μm film spacer (T284, Nitoms, Inc., Tokyo, Japan) was placed between a dye-adsorbed photoelectrodes and a counter electrode. The electrolyte was inserted in the gap of the film spacer using capillary force.

3.4 Photovoltaic Characterizations

Solar energy conversion efficiency and photovoltaic characteristics were investigated under simulated solar light at the standard AM 1.5 (100mW/cm^2) using a solar simulator (XES-40S1, San-Ei Electric, Osaka, Japan). The light intensity of illumination source was calibrated using a standard silicon photodiode (BS520, Bunkoh-Keiki Co. Ltd., Tokyo, Japan). The photocurrent-voltage (*J*-*V*) characteristics of devices were measured by using a source meter (6241A, ADCMT, Tokyo, Japan). FE-SEM was used to investigate the morphology of DSSC photoanodes. UV-vis spectroscopy (UV-3100 PC, Shimadzu, Japan) was used to measure the amount of dye absorption in DSSCs.

CHAPTER 4
RESULTS AND DISCUSSION

4.1 Preparation of TiO_2 Precursor

Titanium alkoxide (TTIP) can be used as a TiO_2 precursor solution as shown in Fig. 4.1. Titanium alkoxide was used instead of conventional TiO_2 sol because titanium alkoxide is molecularly smaller than TiO_2 sol, so titanium alkoxide could be used to synthesize smaller TiO_2 nanostructures. The hydrolysis of titanium alkoxide followed by condensation was involved in this process (Eq. 4.1) [27]. The hydrolysis progressed by the reaction between titanium alkoxide and the water in the atmosphere (relative humidity (RH) between 40%). After insertion of the precursor solution (in all setting methods), AAO membranes were exposed to the air for around 30 min for the proceeding of the hydrolysis reaction. By the hydrolysis reaction, the color of AAO membranes changed into whitish due to the color of TiO_2 after hydrolysis as shown in Fig. 4.2. Then the samples became more whitish after calcination at 450 ^oC (Fig. 4.2 (c)).

(a)

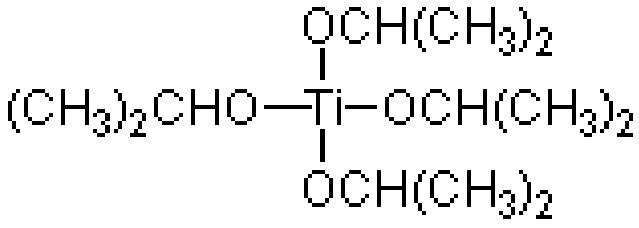

(b)

Fig. 4.1 TTIP: (a) photographical image of prepared TTIP solution using TiO_2 precursor and (b) TTIP molecular structure.

$$C_{12}H_{28}O_4Ti + 2H_2O \text{ (atmosphere)} \rightarrow TiO_2 + 4(CH_3)_2CHOH \qquad (4.1)$$

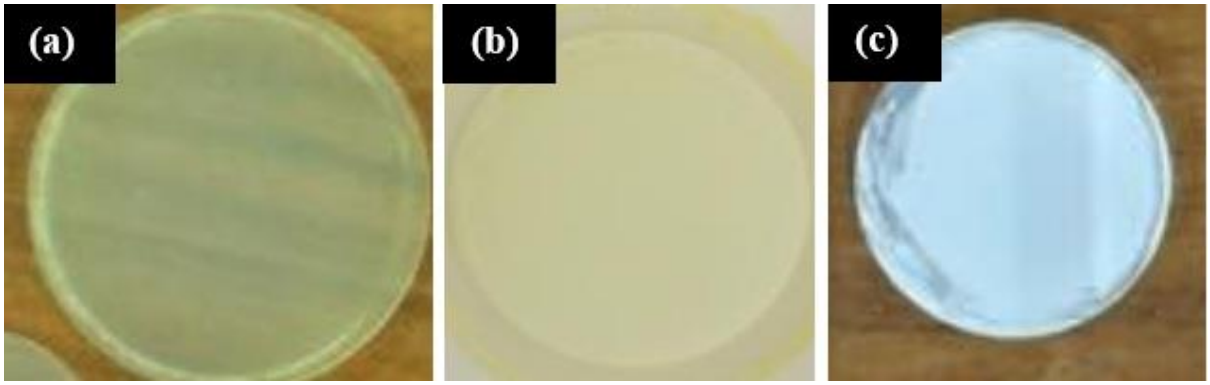

Fig. 4.2. Photographical images of AAO templates (a) after IS setting and then (b) after exposure to the air for 30 min and (c) after calcination at 450 ºC.

In pursuit of TiO_2 nanorods and semi-nanotubes, titanium alkoxide with the addition of 2,4-pentanedione (acetylacetone) was used as the precursor. 2,4-pentanedione was added in order to form a chelate titanium alkoxide. The chelation by the acetylacetone inhibited hydrolysis of titanium alkoxide [16, 27]. Vacuum filtration was used to fill the titanium alkoxide into the center region of the AAO pores. The remaining titanium alkoxide left in the pores was then hydrolyzed by water in atmosphere. The above method above could fabricate TiO_2 nanorods and semi-nanotubes efficiently at room temperature.

4.2 Dissolution of AAO Template

In this research, after calcination, samples were treated by 1 M HCl [16] and 1 M NaOH [28] to remove AAO template from samples. The samples after calcination were put in a centrifuge tube filled with 1 M HCl or 1 M NaOH. Figs. 4.3(a), 4.3(b) and 4.3(c) showed photographical images of HCl treatment. These samples were mildly heat-treated at 40°C for 1, 24, and 72 h, respectively. Samples from 1 M NaOH treatment that left at room temperature for 1 h showed the photographic image was the same as that of the HCl treatment at 72 h (Fig. 4.3(d)).

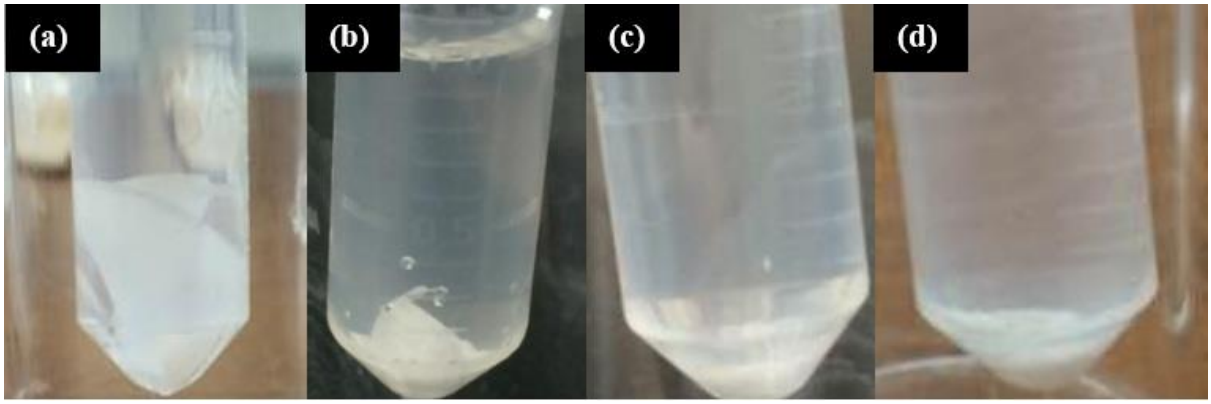

Fig. 4.3 Photographical images of AAO templates that were immersed in HCl for (a) 1 h, (b) 24 h, (c) 72 h, and in NaOH for (d) 1 h.

Fig. 4.4 shows XRD patterns of the samples synthesized by AAO template method~~,~~ using IS (sample with 1M HCl treatment for 0, 1 and 72 h). Without HCl treatment, broad peaks of the amorphous templates (AAO) as well as weak peaks of anatase TiO_2 were observed. With 72 h HCl treatment, the broad peaks of AAO disappeared, and only the peaks of anatase TiO_2 were ~~only~~ observed [16].

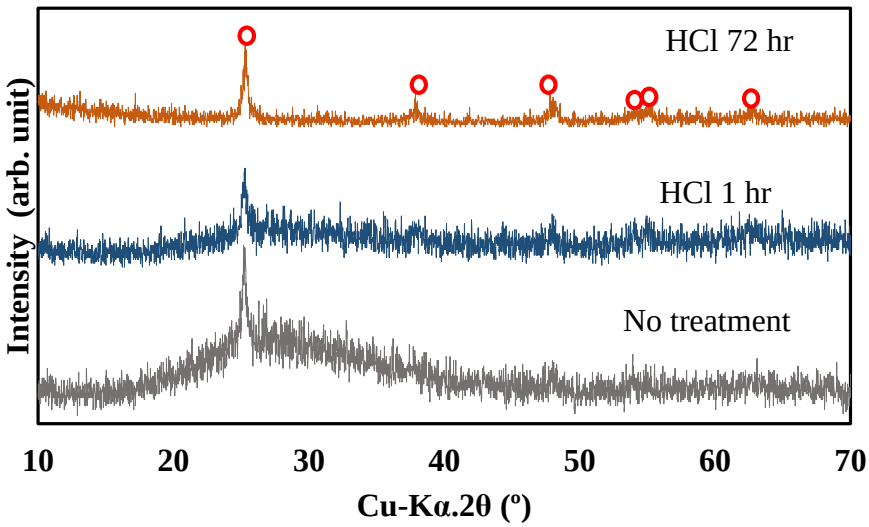

Fig. 4.4 XRD patterns of the samples from IS without HCl treatment (including AAO template) and with HCl treatment to remove the AAO template (1M HCl at 40°C for 1 and 72 h).

Fig.4.5 shows the XRD patterns of the synthesized samples by the AAO template method using IS which were subsequently dissolved in 1 M NaOH for 0, 1 h and >15 h. When time of template dissolution was exceeded 1 h the products which were soluble could be

transported into the solution, The template was removed by the treatment for 1h and then Bayerite ($Al(OH)_3$) was precipitated in the samples by the treatment for >15 h. [34].

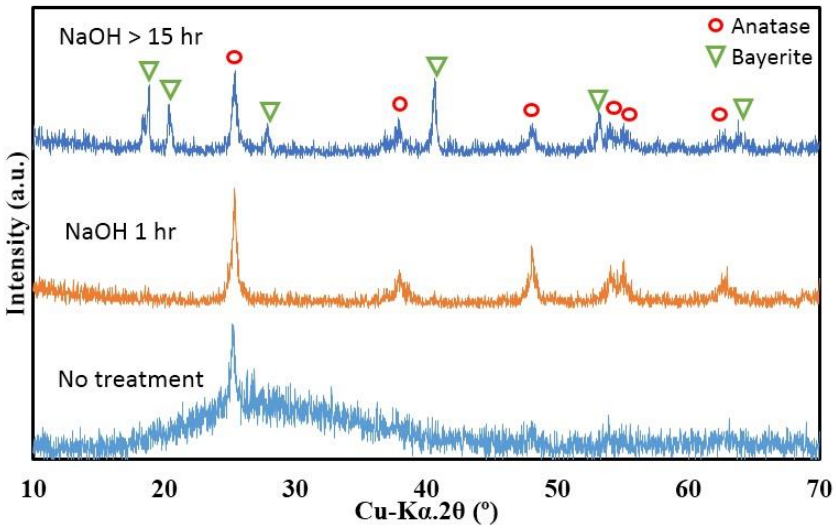

Fig. 4.5. XRD patterns of samples from IS without NaOH treatment (including AAO template) and with NaOH treatment to remove AAO template (1 M NaOH at room temperature for 1 and 15 h).

Fig. 4.6 shows XRD patterns of the samples synthesized by the AAO-template method using IS with/without template dissolution treatments. Without any treatment, weak peaks of anatase TiO_2 were observed with a broad peak of the amorphous AAO template. With 72 h HCl treatment, the broad peak of AAO disappeared, and the peaks of anatase were only observed. This result is in accordance to the previous report [34]. In order to reduce the time of the template dissolution step, NaOH aq. was used instead of HCl aq. The XRD pattern confirmed that for only 1 h in NaOH, it was enough to dissolve AAO template, i.e. only the peaks of anatase TiO_2 were observed in the pattern. The XRD patterns of the samples synthesized by AAO-template method using VDS also showed the same results as using IS.

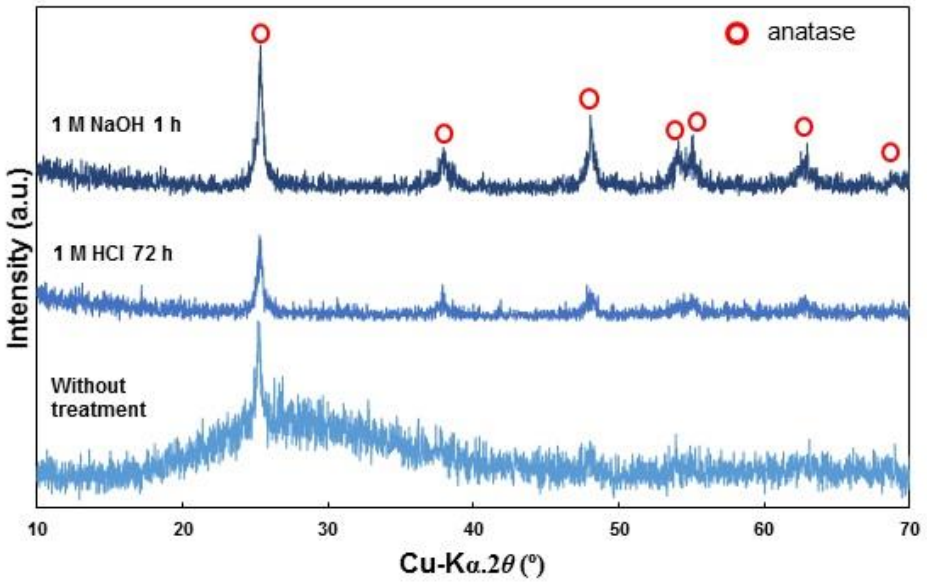

Fig. 4.6. XRD patterns of the samples from IS without treatment (including AAO template) and with treatments (to remove AAO template), using HCl treatment (1 M HCl at 40ºC for 72 h) and NaOH treatment (1 M NaOH at room temperature for 1 h).

4.3 Microstructures of AAO Template, Nanorods, and Semi-nanotubes

4.3.1 AAO template

Commercial AAO templates (with pore diameters of 100 nm and 200 nm) before IS and VDS were characterized by SEM images as shown in Fig. 4.7. Major drawbacks of those commercial templates are the lack of the ordered pore structure, non-uniform pores, and larger sizes than the catalog values of pore diameter [17]. In comparison between templates with a pore diameter of 200 and 100 nm, the former have more uniform pore structure than do the latter.

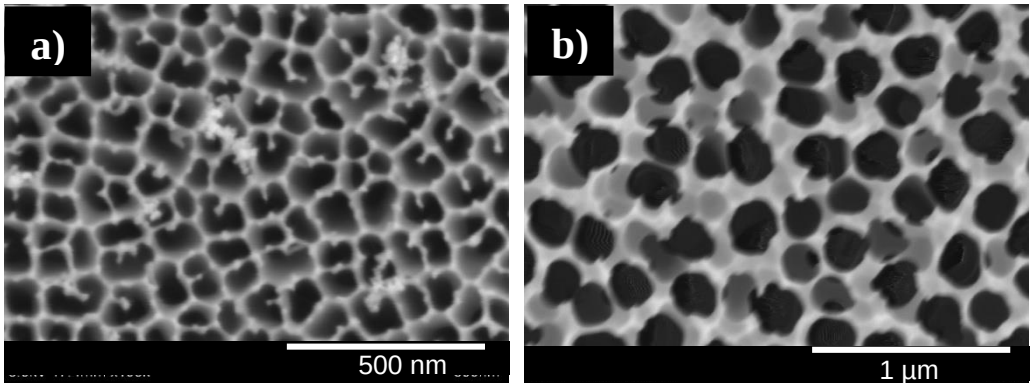

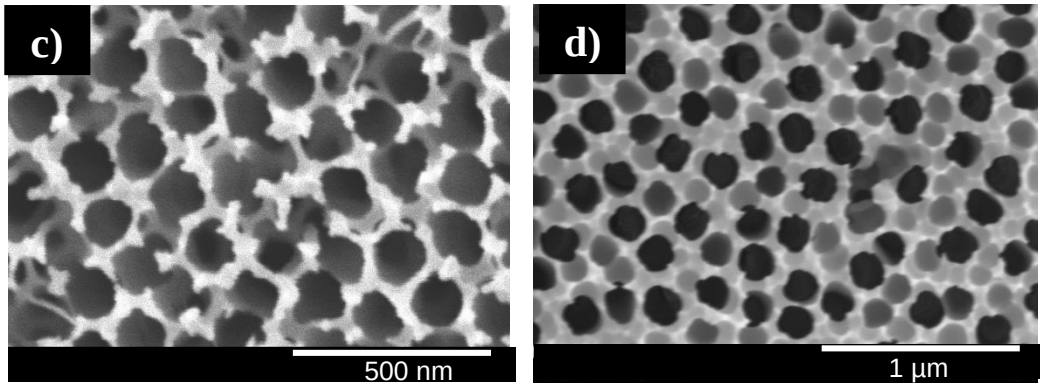

Fig. 4.7 SEM images of pore structure of AAO templates with diameters of (a-b) 100 nm and (c-d) 200 nm.

4.3.2. AAO template with inserted precursor and the synthesized TiO_2 nanorods and semi-nanotubes after dissolution of templates in NaOH aq.

Fig. 4.8(a) confirms that AAO template declared the pore diameter of 100 nm; nevertheless, there was only a thin top surface layer with the pore diameter of 100 nm and thick bottom layer had the pore diameter of 200 nm.

Fig.4.8 (b), shows the AAO template from ISunder only low vacuum to help the precursor to penetrate into the template pores. So, there were some part of TiO_2 struck on the surface and some penetrated into the pores. When a commercial 100 nm-grade AAO template was immersed in TiO_2 precursor solution and dissolved in NaOH solution, the 1-D structured TiO_2 nanorods with a diameter of 100-200 nm and a length of 1-2 µm were observed as shown in Figs. 4.9(a), 4.9(b), and 4.9(c). The commercial AAO template used in this work is normally used as a liquid filter, so its pore diameters are not uniform through the 1-D pore channels [19, 17]. The template has diameters of 100 and 200 nm at the top and the bottom, respectively, as shown in Fig. 4.9(a). The thickness of the filter layer with a pore diameter of 100 nm is only about 2 µm on top of the template (Fig. 4.9(b)). Therefore, the nanorods with varied diameter between 100 and 200 nm were obtained from this method. Apart from TiO_2 nanorods obtained after dissolution of AAO template, a formation of some TiO_2 nanoparticles was also revealed in Fig. 4.9(c).

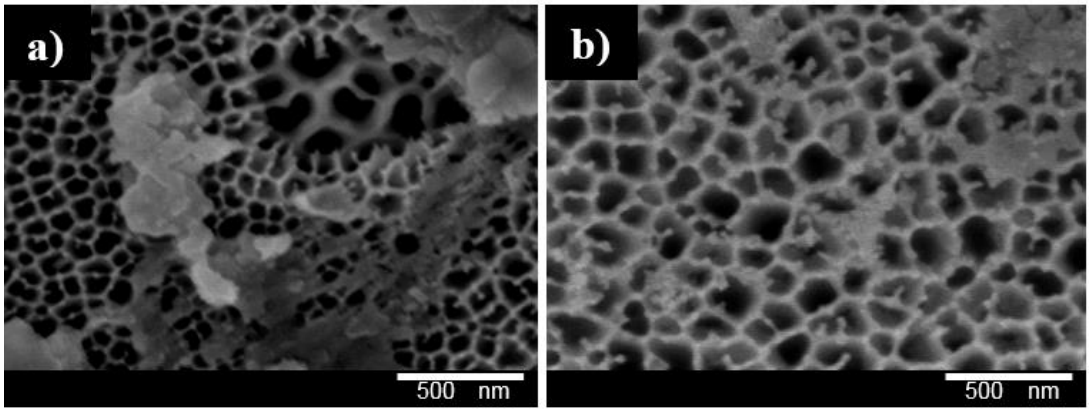

Fig. 4.8 SEM images of IS: (a) filtered side with some broken parts of AAO template and (b) TiO_2 penetrated in pore and stuck on the surface.

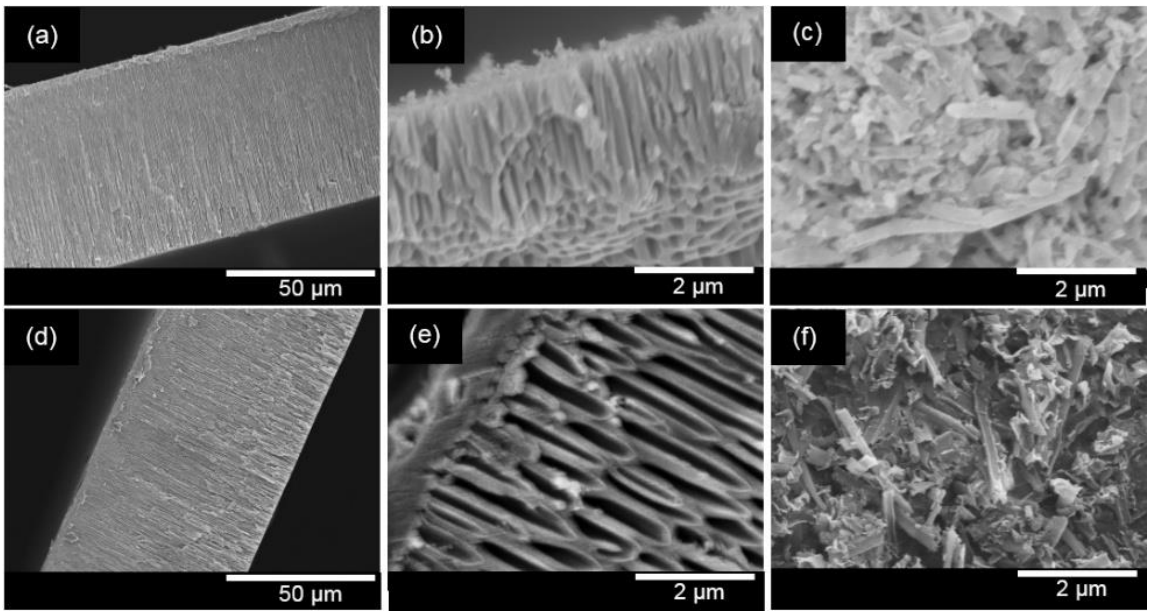

Fig. 4.9 SEM images of (a) side face of 100 nm-grade AAO template used in IS, (b) filter layer of 100 nm-grade AAO template, (c) synthesized nanorods via IS after dissolution of AAO template, (d) side surface of 200 nm-grade AAO template used in VDS, (e) filter layer of 200 nm-grade AAO template, and (f) synthesized semi-nanotube structure via VDS after AAO dissolution.

For a commercial 200 nm-grade AAO template, TiO_2 precursor was dropped on the template under higher vacuum to help the TiO_2 precursor solution to penetrate~~d~~ into the pores in VDS as shown in Figs. 4.9(d)-(f). After dissolution of AAO template in NaOH, the 1-D structured TiO_2 semi-nanotubes with a diameter of 100-200 nm and a length of 5-10 μm were

observed (Fig. 4.9(f)). This type of nanostructure might be obtained by the severe NaOH treatment for TiO_2 in AAO template which induced ~~trans~~formation of nanotubes [28] instead of nanorods [16]. This was also affected by the higher vacuum used in VDS. The TiO_2 nanostructure from VDS was different from that of IS, so it is confirmed that the morphology of nanostructured TiO_2 as diameter and length can be adjusted by changing the sample setting [11, 16, 17].

4.4 DSSC Fabrication

In this research, only the open cell structure was fabricated for characterization as indicated in Fig. 4.10. The open cell structure is easy to fabricate, measure, and characterize. The area of the cells was 1x1 cm^2 and measured by ImageJ software for all samples.

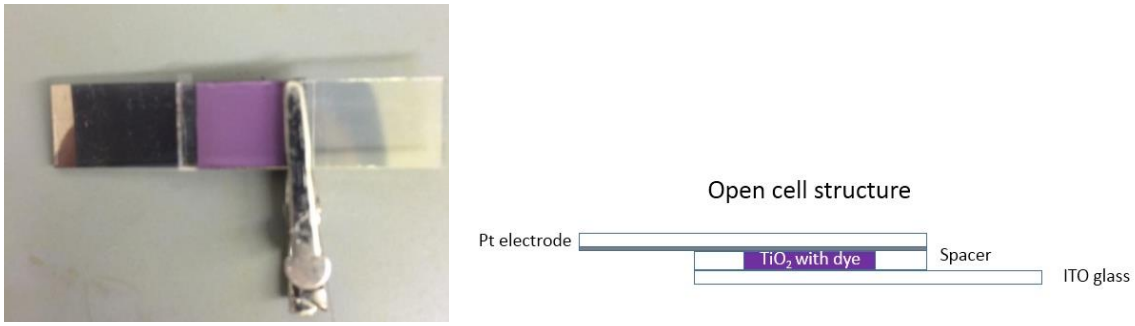

Fig. 4.10 Photographical images of open cell structure

4.4.1 XRD pattern of mixed paste

Mixed pastes of nanorods (or semi-nanotubes) and nanoparticles were characterized by XRD to confirm only that TiO_2 phase existed in the paste. Fig. 4.11 shows XRD patterns of mixed pastes before and after calcination. Both from IS and VDS showed the same results that only peaks from TiO_2 (anatase and rutile) appeared. The observed rutile peaks came from commercial nanoparticle (P25) used in this research. No trace of another phase was observed.

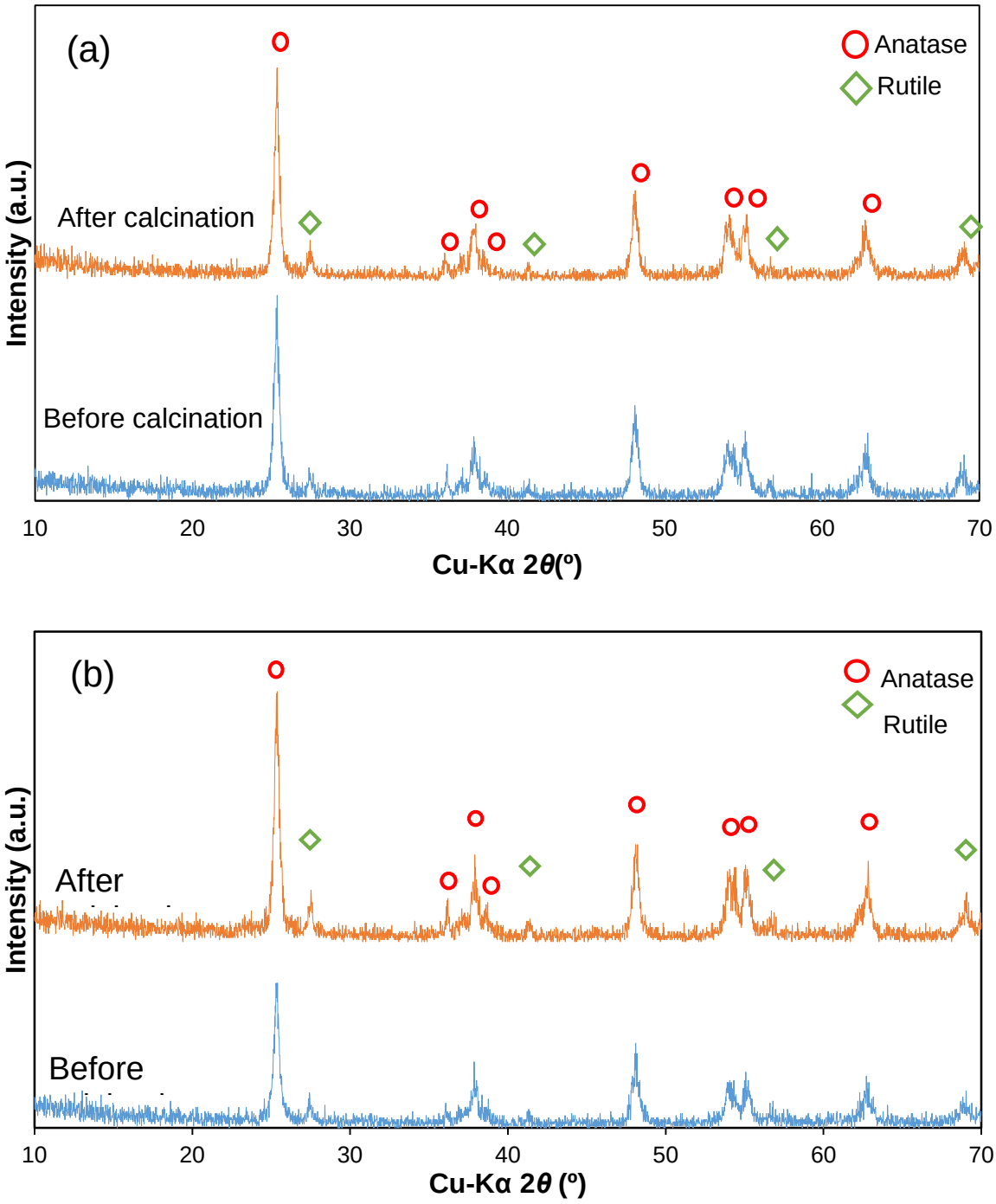

Fig. 4.11. XRD patterns of mixed paste of nanoparticles and (a) nanorods fabricated from IS and (b) semi-nanotubes fabricated from VDS before and after calcination at 450 º C.

Fig. 4.12 shows EDS spectra of synthesized TiO_2 nanorods from IS. It was found that after dissolution in NaOH aq., only titanium and oxygen elements remained in nanomaterials in both wide and specific areas. The carbon signal came from contamination. These results

confirmed again the availability of dissolution treatment of AAO template in NaOH, which is in a good agreement with XRD results.

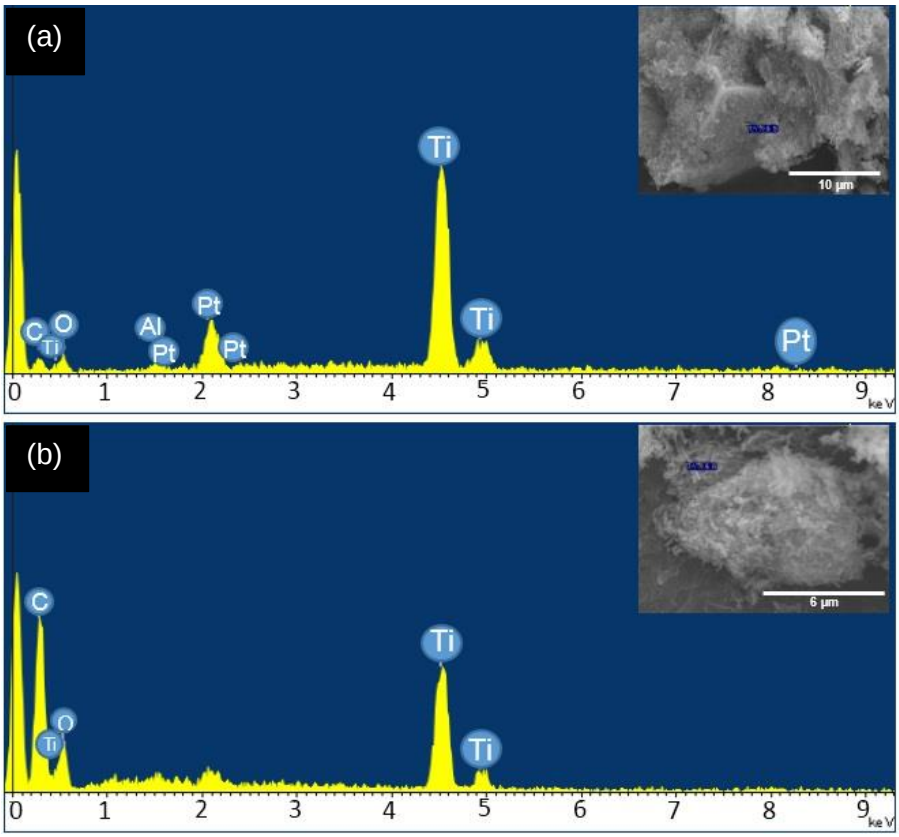

Fig. 4.12 EDS spectra of synthesized TiO_2 nanorods from IS at (a) wide and (b) specific areas. Insets indicate analysis positions in SEM images.

4.5 Photovoltaic Characterizations

4.5.1 Photovoltaic characterizations of DSSCs made of nanorods from IS

Fig. 4.13 shows *J-V* characteristics of DSSCs fabricated using pristine TiO_2 nanoparticles (for comparison) and mixtures of TiO_2 nanorods/nanoparticles (NR/NP) at ratio of 5:95, 10:90 and 15:85 (by weight). When the TiO_2 nanorod/nanoparticle electrode was used, *PCE* of the cell increased to 4.68%, while that ~~of~~ was only 4.28% for the system composed of the pristine TiO_2 nanoparticles.

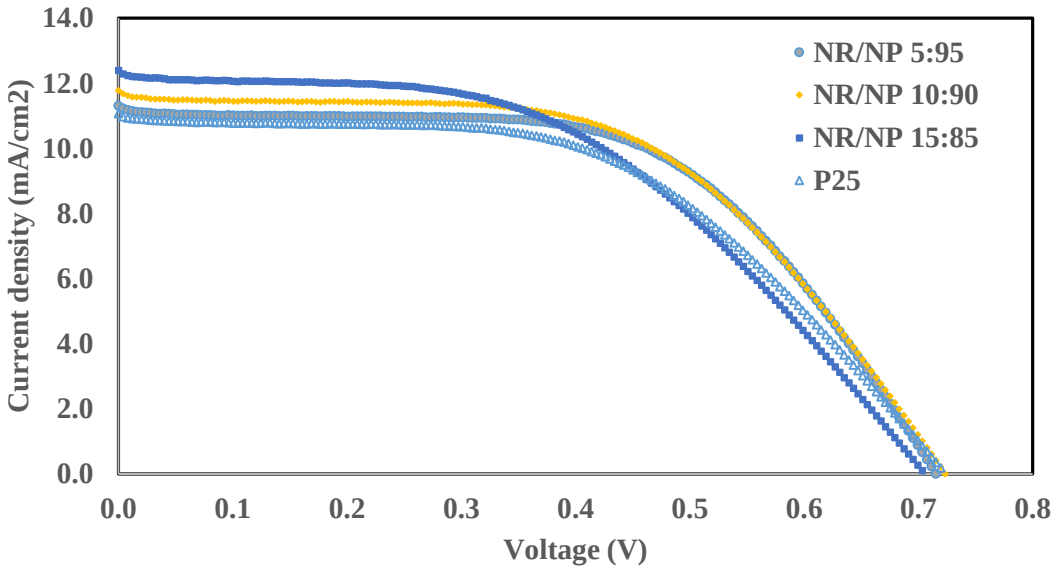

Fig. 4.13 *J-V* characteristics of DSSCs fabricated using pristine TiO_2 nanoparticles and ~~mixed~~ mixture of TiO_2 nanorods/nanoparticles at ratio of 5:95, 10:90 and 15:85 (by weight).

Although the specific surface area of the nanorods is lower than that of nanoparticles, the photo-generated electron can directly move along the 1-D ordered structure to conducting glass with reducing the possible loss of photoelectrons and increasing the performance of the cell. On the contrasy, the previous work suggested that addition of nanorods into nanoparticles system might decrease the total specific surface area [2, 4, 28]. Therefore, a proper content of nanorods supplement into nanoparticles may effectively increase the performance of DSSCs as shown in Table 4.1. The average thickness was measured by SEM image of samples.

Table 4.1 Cell performances of DSSC from nanoparticles (P25) and DSSC from nanorods (NR)/ nanoparticles (NP) mixture (film thickness of ~20 μm).

Sample	J_{sc} (mA/cm^2)	V_{oc} (V)	*FF*	Efficiency (%)
1 layer TiO_2 NP	11.07	0.72	0.53	4.28
1 layer TiO_2 NR/NP (5:95)	11.17	0.72	0.57	4.68
1 layer TiO_2 NR/NP (10:90)	10.88	0.71	0.54	4.21
1 layer TiO_2 NR/NP (15:85)	11.15	0.71	0.52	4.07

4.5.2 UV-vis spectra of NR/NP photoanodes

To investigate the amount of dye adsorption in photoanodes, the adsorbed dye was dissolved by HCl solution. The UV-vis spectra of dissolved dye solution from 2 types of TiO_2 nanostructures, i.e. TiO_2 nanoparticles (NP) and TiO_2 nanorods/nanoparticles (NR/NP = 5:95), were obtained as shown in Fig. 4.14. The absorption band is at approximately 500 nm. In the spectra of the nanorods/nanoparticle, the dye absorption bands of NR/NP were slightly higher in compared with those of the P25 sample. The UV-vis spectra show that more effective photon capturing is achieved in the visible light region in the NR/NP cell because more N719 dyes can be adsorbed onto the film [50].

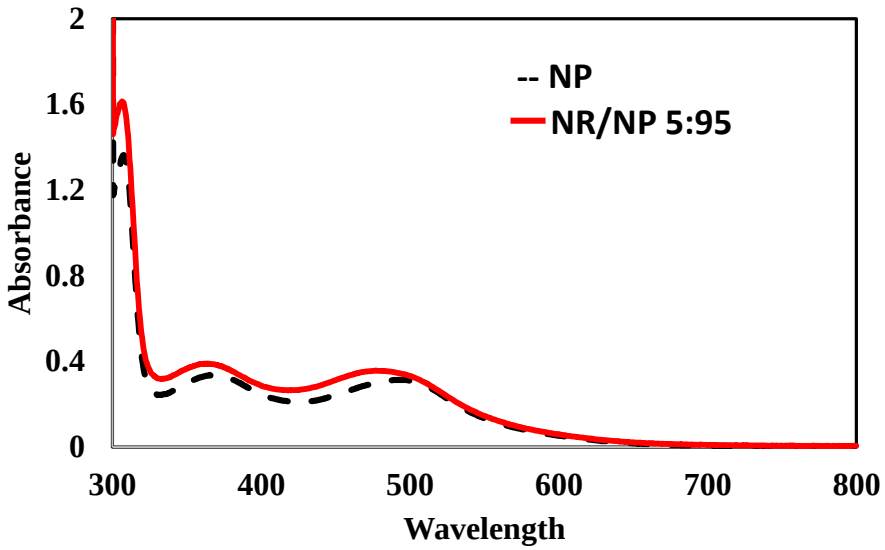

Fig. 4.14 UV-vis spectra shows the amounts of dye adsorptions in a NR/NP cell (5:95 by weight) (NR from IS) and a NP cell for comparison.

4.5.3 SEM images of NR/NP Photoanodes

Fig. 4.15 shows ~~a~~ SEM images of the photoelectrode fabricated from mixed TiO_2 NR/NP (5:95 by mass fraction), showing some nanorods bridged with small nanoparticles. This morphology is appropriate for a good electron conducting pathway and some bridged nanowires provide the interconnections via anchoring effect, which can help to reduce charge recombination in photocathodes [4, 7, 28].

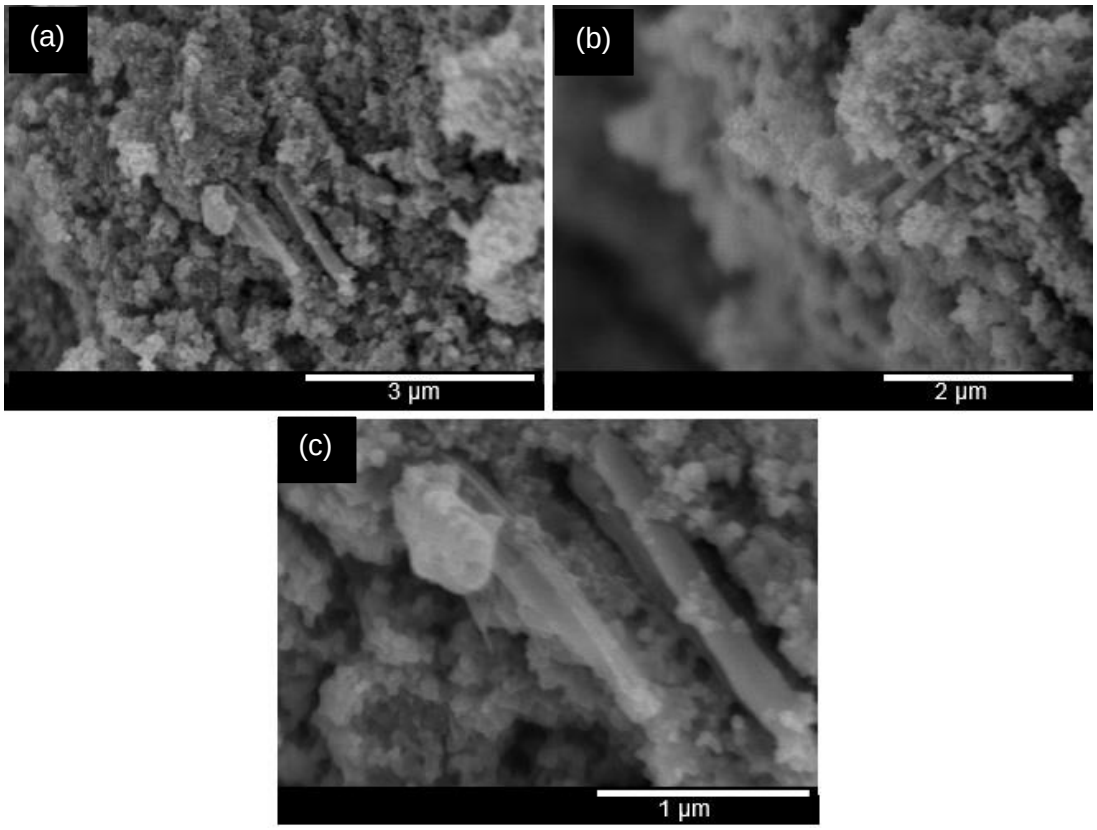

Fig. 4.15 Bridging between nanorods and nanoparticles.

Fig. 4.16 presents a series of SEM observations. It can be deduced that a mixing process only by magnetic stirring resulted in agglomerations of nanorods. The particle and synthesized nanorods were separated in the paste (Figs. 4.14(a), 4.14(b) and 4.14(c)) and the 1-layer coating using this paste lead to many crack formations on the surface (Fig. 4.14(d)).

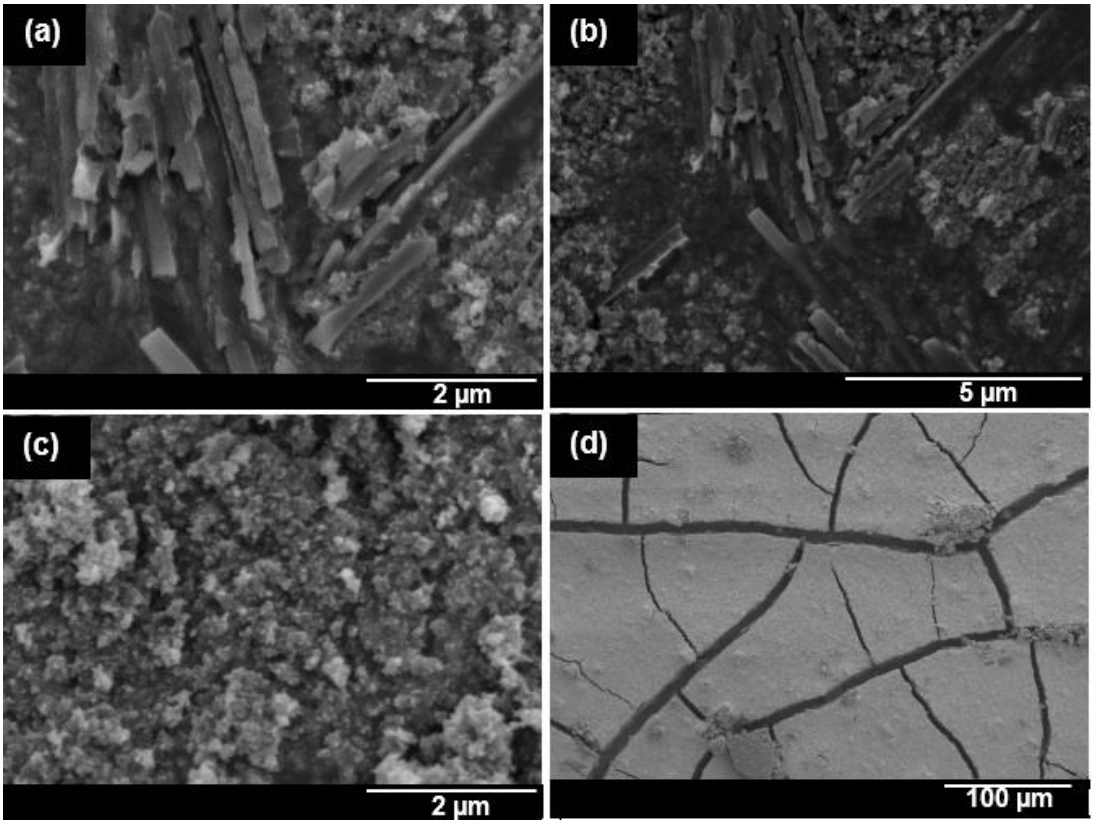

Fig. 4.16 SEM image of (a-c) TiO_2 nanorods/nanoparticles paste with DSSCs electrodes and (d) cracks on electrode surface after being calcined at 450 ºC

4.5.4 SEM images and photovoltaic characterizations of DSSCs made of semi-nanotubes from VDS

After VDS setting, template was dissolved in 1 M NaOH for 1 h. Semi-nanotube structures appeared after dissolution of the template as showed in Fig. 4.17. It was significant different from that from IS. This result confirmed that the TiO_2 nanostructure could be controlled by changing the setting method.

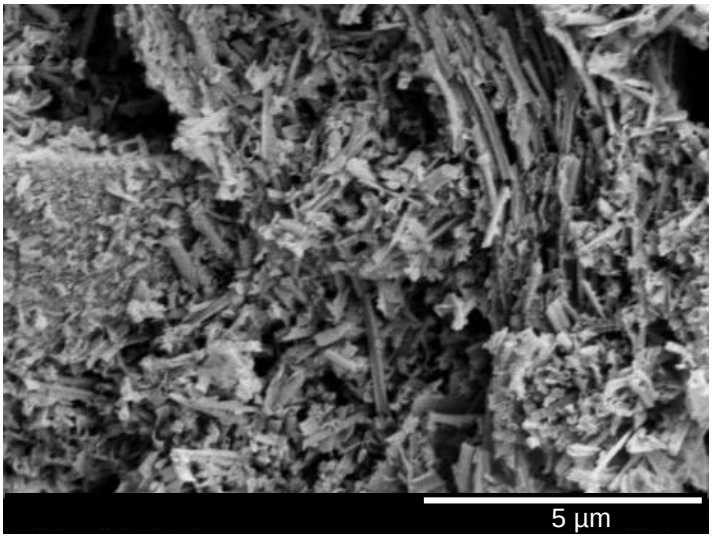

Fig. 4.17 A SEM image of TiO_2 semi-nanotube, structure after template dissolution from VDS.

Improvement of mixing method by using sonication and magnetic stirrer leads to the better dispersion of TiO_2 semi-nanotube as revealed in Figs. 4.18(a) and 4.18(c). Although, this technique could help~~ed~~ to improve dispersion, some agglomeration of TiO_2 semi-nanotube still occurred (Fig. 4.18(b)). coating of paste DSSCs electrode reduced cracking on the surface (Fig. 4.18(d)).

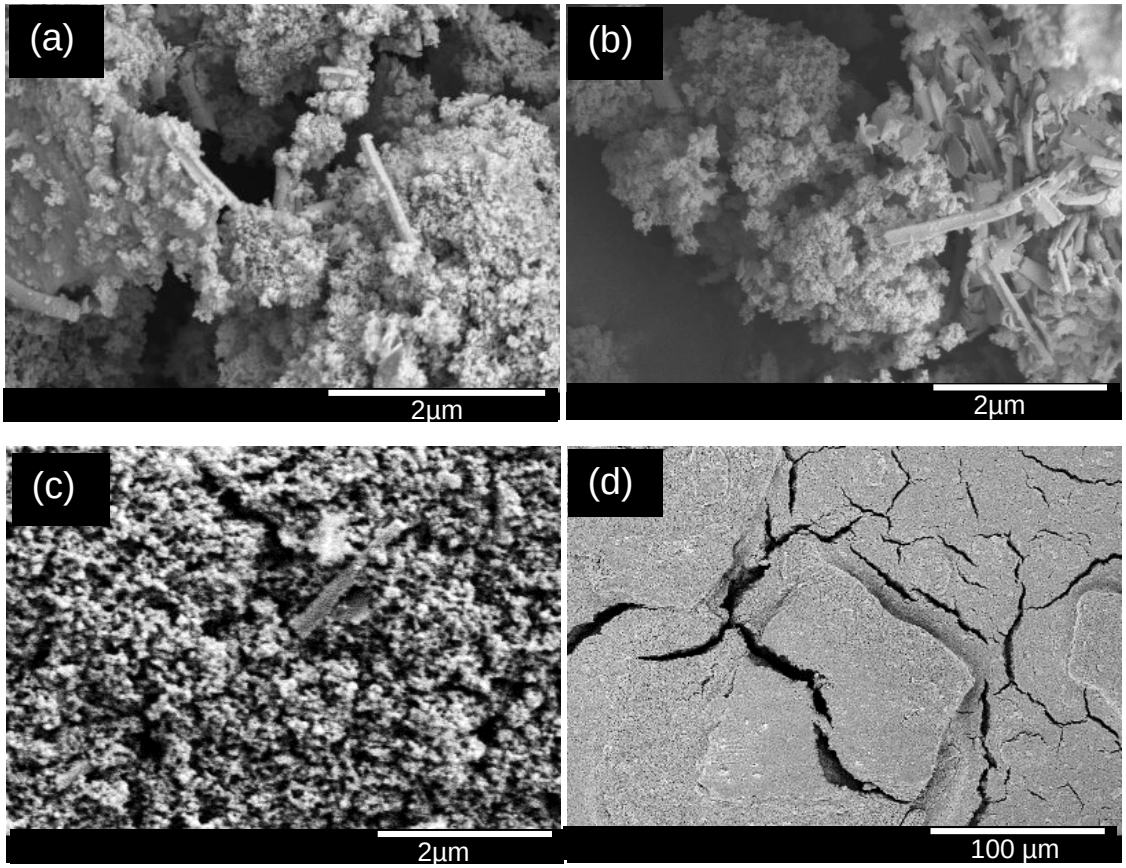

Fig. 4.18. SEM images of TiO_2 paste of using semi-nanotubes (SNT) from VDS: (a), (b)-after mixing with NP via magnetic stirrer and sonication , (c) dispersion of semi-nanotubes after 2-layer coating on electrode and (e) small cracks on electrode surface.

4.5.5 Effect of coating layer on performances of DSSCs made of semi-nanotubes

With improved mixing process and 2-layer coating, the PCE had clearly improved from 4.11% to 4.77%, as shown in Table 4.2. The better dispersion of synthesized semi-nanotubes and less crack on the surface improved charge transport, gave more adhesion and bridging between nanoparticle and synthesized semi-nanotubes [34]. Furthermore, the results can attribute to further advantages of synthesized nanostructures. The obtained length of synthesized semi-nanotubes did not exceed 10 µm, which could help to improve PCE [51].

Table 4.2. Cell performances of DSSCs from nanoparticles (NP) and DSSC from semi-nanotubes (SNT)/ nanoparticles (NP) mixture (1 coating with film thickness of ~20 μm and 2 coating with film thickness of ~30 μm).

Sample	J_{sc} (mA/cm^2)	V_{oc} (V)	FF	Efficiency (%)
1 layer TiO_2 NP	11.07	0.72	0.53	4.28
1 layer TiO_2 SNT/NP (5:95)	11.20	0.71	0.56	4.58
1 layer TiO_2 SNT/NP (10:90)	11.27	0.74	0.56	4.68
1 layer TiO_2 SNT/NP (15:85)	10.37	0.70	0.52	4.17
2 layer TiO_2 NP	10.61	0.72	0.55	4.17
2 layer TiO_2 SNT/NP (5:95)	11.72	0.70	0.51	4.20
2 layer TiO_2 SNT/NP (10:90)	10.65	0.73	0.61	4.75
2 layer TiO_2 SNT/NP (15:85)	9.61	0.73	0.52	3.82
2 layer TiO_2 NP	10.61	0.72	0.55	4.17
1 layer TiO_2 + 1 layer SNT/NP (5:95)	12.82	0.70	0.48	4.27
1 layer TiO_2 + 1 layer SNT/NP (10:90)	11.92	0.70	0.57	4.77
1 layer TiO_2 + 1 layer SNT/NP (15:85)	11.84	0.72	0.55	4.69

4.5.6 UV-vis spectra of photoanodes made of semi-nanotubes

Fig. 4.19 shows UV-vis spectra indicating the absorption of dye on DSSC electrodes. For the 1-layer coated electrode, only NP had the highest dye absorption because of its larger surface area (Fig. 4.19(a)). In contrast, for the synthesized nanostructures mixed with nanoparticles (NR/NP or SNT/NP) even coated with 1 or 2 layers, dye absorption decreased due to their smaller surface areas. Although the specific surface area of nanorods or semi-nanotubes are lower than nanoparticles, the photo-generated electron can move more efficients along the 1-D structure to conducting glass with reducing the possible loss of photoelectron and increasing the performance of the cell.

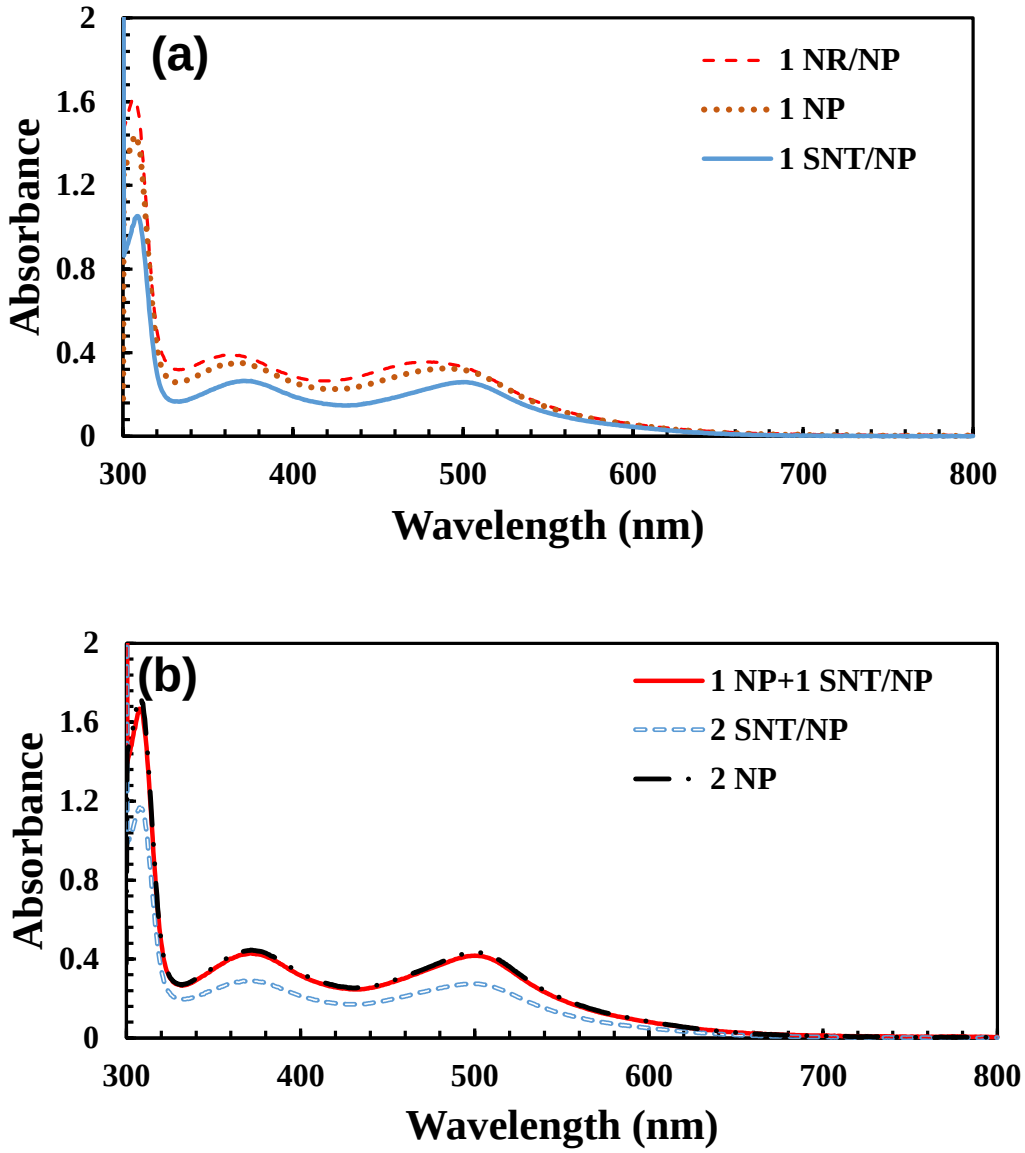

Fig. 4.19 UV-vis spectra show dye absorption in (a) 1-layer coated photoanodes of NR/NP, NP, and SNT/NP; and (b) 2-layer coated photoanodes with different coating patterns.

CHAPTER 5
CONCLUSION

In this thesis, nanorods/semi-nanotubes TiO_2 were fabricated and applied in DSSCs. They were characterized by XRD, SEM, solar simulator, and UV-vis. Obtained nanorods/semi-nanotubes were mixed with nanoparticles and used as photocathodes in DSSCs. Their DSSC performances were compared between these 2 types of structures and also conventional cells made of pristine nanoparticles. The results are summarized as follows:

1. TiO_2 can be successfully synthesized by immersion setting (IS) and vacuum drop setting (VDS) (calcined at 450ºC for 1 h). With the calcination and NaOH aq. treatment to remove AAO, SEM characterization revealed that TiO_2 nanorods with diameters around 100-200 nm were successfully fabricated from IS, whereas TiO_2 semi-nanotubes with 200 nm pore diameter were successfully fabricated from VDS.

2. The length of semi-nanotubes did not exceed 10 μm because of the shrinkage by heat treatment, NaOH aq. treatment, and magnetic stirring.

3. The synthesized nanorods mixed with commercial TiO_2 nanoparticles (NP) and the synthesized semi-nanotubes mixed with NP have optimum mixing ratios at 5:95 and 10:90 (by mass), respectively. The photoelectrodes made with nanorods or semi-nanotubes showed better performances than did the cells of only NP. Due to the 1-D nanostructure dispersion, the electron expressway concept was effective in this research.

RECOMMENDATIONS

1. The results that obtained from scanning electron microscopy (SEM) showed that completed nanowire structures still cannot be obtained from VDS because of high vacuum. Therefore, the condition to achieve this objective should be more optimized.
2. The size of the commercial AAO filter in this work was too small for the fabrication of nanomaterials. Only small yield of products could be achieved. Wide area AAO template should be synthesized or purchased for mass production of TiO_2 nanomaterials.
3. Characterizations of scattering layers are needed to confirm theirs effects on DSSC.
4. Other characterization techniques are needed for the investigations of DSSC, such as, incident photons to current efficiency (IPCE), impedance measurements, and transmittance of cells.

REFERENCES

[1] B. O'Regan and M. Gratzel "A low cost, high efficiency based on dye-sensitized colloidal TiO_2 films" **Nature**, 353 (1991), 737.

[2] Y. Ding, L.E. Mo, L. Tao, Y.M. Ma, L.H. Hu, Y. Huang, X.Q. Fang, J.X. Yao, X.W. Xi, S.Y. Dai, "TiO_2 nanocrystalline layer as a bridge linking TiO_2 sub-microspheres layer and substrates for high-efficiency dye-sensitized solar cells" **Journal of Power Sources**, 272 (2014), 1046-1052.

[3] Y. Okamoto and Y. Suzuki, **"**Perovskite-type SrTiO3, CaTiO3 and BaTiO3 porous film electrodes for dye-sensitized solar cells**" Journal of the Ceramic Society of Japan**, 122, 728-731 (2014).

[4] Y. Suzuki, S. Ngamsinlapasathian, R. Yoshida, S. Yoshikawa "Partially nanowire-structured TiO_2 electrode for dye-sensitized solar cells" **Central European Journal of Chemistry**, 4 (3) (2006), 476-488.

[5] A. Yella, H. W. Lee, H. N. Tsao, C. Yi, A. K. Chandiran, M. K. Nazeeruddin, E. W. G. Diau, C. Y. Yeh, S. M. Zakeeruddin, M. Grätzel "Porphyrin Sensitized Solar Cells with Cobalt (II/III)–Based Redox Electrolyte Exceed 12 Percent Efficiency" **Science**, 334 (2011), 629.

[6] S. Ito, T.N. Murakami, P. Comte, P. Liska, C. Grätzel, M. K. Nazeeruddin , M. Grätzel, "High-Efficiency Organic-Dye-Sensitized Solar Cells Controlled by Nanocrystalline-TiO2 Electrode Thickness" **Thin Solid Films**, 516 (2006), 4613–4619.

[7] K. Asagoe, S. Ngamsinlapasathian, Yoshikazu Suzuki, Susumu Yoshikawa "Addition of TiO_2 nanowires in different polymorphs for dye-sensitized solar cells" **Central European Journal of Chemistry**, 5 (2) 2007 605–619.

[8] D. Kuang, J. Brillet, P. Chen, M. Takata, S. Uchida, H. Miura, K.Sumioka, S. M. Zakeeruddin, and M. Grätzel "Application of Highly Ordered TiO_2 Nanotube Arrays in

Flexible Dye-Sensitized Solar Cells" **American Chemical Society**, 2 (6) (2008), 1113–1116.

[9] E. Stathatos "Dye Sensitized Solar Cells: A New Prospective to the Solar to Electrical Energy Conversion. Issues to be solved for Efficient Energy Harvesting." **Journal of Engineering Science and Technology Review**, 5 (2012), 9-13.

[10] S. Chuangchote, T. Sagawa, S. Yoshikawa, "Efficient dye-sensitized solar cells using electrospun TiO_2 nanofibers as a light harvesting layer" **Applied Physic Letter**, 93 (2008), 033310.

[11] X. Chen and S. S. Mao "Titanium Dioxide Nanomaterials: Synthesis, Properties, Modifications, and Applications" **Chemical Review**, 107 (2007), 2891-2959.

[12] B. Liu and E. S. Aydil "Growth of Oriented Single-Crystalline Rutile TiO2 Nanorods on Transparent Conducting Substrates for Dye-Sensitized Solar Cells" **American Chemical Society**, 131 (2009), 3985–3990.

[13] S. Sadhu, and P. Poddar "Template-Free Fabrication of Highly-Oriented Single-Crystalline 1D Rutile TiO2-MWCNT Composite for Enhanced Photoelectrochemical Activity" **Journal of Physic Chemistry C**, 118 (2014), 19363−19373.

[14] Q. Hu, C. Wu, L. Cao, B. Chi, J. Pu, L. Jian "A novel TiO_2 nanowires/nanoparticles composite photoanode with SrO shell coating for high performance dye-sensitized solar cell" **Journal of Power Sources**, 226 (2013), 8-15.

[15] J. Huang, S. Chiam, H. Tan, S. Wang and W. K. Chim, "Fabrication of Silicon Nanowires with Precise Diameter Control Using Metal Nanodot Arrays as a Hard Mask Blocking Material in Chemical Etching" **Chemical Material**, 22 (2010), 4111–4116.

[16] K. Aisu, T. S. Suzuki, E. Nakamura, H. Abe and Y. Suzuki "AAO-template assisted synthesis and size control of one-dimensional TiO_2 nanomaterials**"** **Journal of the Ceramic Society of Japan**, 121 (2013), 915-918.

[17] G. D. Sulk, L. Zaraska, W.J.Stepniowski "Anodic Porous Alumina as a Template for Nanofabrication" **Encyclopedia of Nanoscience and Nanotechnology**, 10 (2009), 1-89.

[18] Y. Lei, W. Cai, G. Wilde "Highly ordered nanostructures with tunable size, shape and properties: A new way to surface nano-patterning using ultra-thin alumina masks" **Progress in Materials Science**, 52 (2007) 465–539.

[19] S. Shingubara "Fabrication of nanomaterials using porous alumina templates" **Journal of Nanoparticle Research**, 5 (2003), 17–30.

[20] Y. Wang, Y. Sun, K. Li "Dye-sensitized solar cells based on oriented ZnO nanowire-covered TiO_2 nanoparticle composite film electrodes" **Materials Letters**, 63 (2009) 1102-1104.

[21] J. Wang, T. Zhang, D. Wang, R. Pan, Q. Wang, H. Xia "Improved morphology and photovoltaic performance in TiO_2 nanorod arrays based dye sensitized solar cells by using a seed layer" **Journal of Alloys and Compounds**, 551 (2013), 82-87.

[22] P. Zhong, W. Que, Y. Liao, J. Zhang, X. Huc "Improved performance in dye-sensitized solar cells by rationally tailoring anodic TiO_2 nanotube length" **Journal of Alloys and Compounds**, 540 (2012) 159–164.

[23] Y. Li, D. Xu, Q. Zhang, D. Chen, F. Huang, Y. Xu, G. Guo and Z. Gu "Preparation of Cadmium Sulfide Nanowire Arrays in Anodic Aluminum Oxide Templates" **Chemical Material**, 11 (1999), 3433-3435.

[24] K. Takahashi, Y.Wang, K. Lee, G. Cao "Fabrication and Li+-intercalation properties of V_2O_5-TiO_2 composite nanorod arrays" **Applied Physics A**, 82 (2006), 27–31.

[25] J. Lee, K. Hong, K. Shin, J. Jho "Fabrication of dye-sensitized solar cells using ordered and vertically oriented TiO_2 nanotube arrays with open and closed ends" **Journal of Industrial and Engineering Chemistry**, 18 (2012), 19-23.

[26] T. Wen, J. Zhang, T. P. Chou, S. J. Limmer and G. Cao "Template-Based Growth of Oxide Nanorod Arrays by Centrifugation" **Journal of Sol-Gel Science and Technology**, 33 (2005), 193–200.

[27] S. Lee, C. Jeon and Y. Park "Fabrication of TiO_2 Tubules by Template Synthesis and Hydrolysis with Water Vapor" **Chemical Material**, 16 (2004), 4292-4295.

[28] C. C. Tsai and H. Teng, "Structural Features of Nanotubes Synthesized from NaOH Treatment on TiO_2 with Different Post-Treatments" **Chemical Material**, 18 (2006), 367-373.

[29] L. Chen, X. Li, L. Qu, C. Gao, Y. Wang, F. Teng, Z. Zhang, X. Pan, E. Xie "Facile and fast one-pot synthesis of ultra-long porous ZnO nanowire arrays for efficient dye-sensitized solar cells" **Journal of Alloys and Compounds**, 586 (2014) 766–772.

[30] G. K. Mor, O. K. Varghese, M. Paulose, K. Shankar, C. A. Grimes "A review on highly ordered, vertically oriented TiO_2 nanotube arrays: Fabrication, material properties, and solar energy applications" **Solar Energy Materials & Solar Cells** 90 (2006) 2011–2075.

[31] G. Tian, K. Pan, Y. Chen, J. Zhou, X. Miao, W. Zhou, R. Wang , H. Fu "Vertically aligned anatase TiO2 nanowire bundle arrays: Use as Pt support for counter electrodes in dye-sensitized solar cells" **Journal of Power Sources**, 238 (2013) 350-355.

[32] A. B. F. Martinson, J. W. Elam, J. T. Hupp and M. J. Pellin *"*ZnO Nanotube Based Dye Sensitized Solar Cells*"* **Nano Letters**, 7 (2007), 2183-2187.

[33] A. B. F. Martinson, J. W. Elam, J. Liu, M. J. Pellin, T. J. Marks, and J. T. Hupp "Radial electron eollection in dye-sensitized solar cells" **Nano Letters**, 8 (2008), 2862-2866.

[34] M. Nukunudompanich, S. Chuangchote, J. Wootthikanokkhan, and Y. Suzuki, "TiO_2 Nanorods Prepared from Anodic Aluminum Oxide Template and Their Applications in Dye-Sensitized Solar Cells" **International Letters of Chemistry, Physics and**

Astronomy, 7 (2015), 30-36.

[35] A. Hagfeldt, G.Boschloo, L. Sun, L. Kloo and H. Pettersson "Dye-Sensitized Solar Cells" **Chemical Reviews**, 110 (11) (2010), 6595-6663.

[36] J. Gong, J. Liang, K. Sumathy "Review on dye-sensitized solar cells (DSSCs): Fundamental concepts and novel materials" **Renewable and Sustainable Energy Reviews**, 16 (2012), 5848-5860.

[37] M. Grätzel "Dye-sensitized solar cells" **Journal of Photochemistry and Photobiology C: Photochemistry Reviews**, 4 (2003), 145-153.

[38] T. Rattanavoravipa, P. Chareonsirithavorn, T. Sagawa and S. Yoshikawa "Efficient electron transfers in ZnO nanorod arrays with N719 dye for hybrid solar cells" **Solid-State Electronics**, 53 (2009), 176-180.

[39] Z. S. Wang , H. Kawauchi b, T. Kashima b, H. Arakawa "Significant influence of TiO_2 photoelectrode morphology on the energy conversion efficiency of N719 dye-sensitized solar cell" **Coordination Chemistry Reviews,** 248 (2004), 1381-1389.

[40] A. C. Nwanya, F. I. Ezema, and P. M. Ejikeme "Dyed sensitized solar cells: A technically andeconomically alternative concept to p-n junction photovoltaic devices" **International Journal of the Physical Sciences**, 6 (22) (2012), 5190-5201.

[41] E. Fortunato, D. Ginley, H. Hosono and D. C. Paine "Transparent Conducting Oxides for Photovoltaics" **Materials Research Society Bulletin**, 32 (2007).

[42] H. Chen and L. Wang "Nanostructure sensitization of transition metal oxides for visible-light photocatalysis" **Beilstein Journal of Nanotechnology**, 5 (2014), 696–710.

[43] S. Ojah, R. G. Nair and S. K. Samdarshi "Recent development in Dye-Sensitized Solar Cells" **Renewable Energy Akshay Urja**, 7 (2013).

[44] Q. Zhang, G.Cao "Nanostructured photoelectrodes for dye-sensitized solar cells" Nano Today, 6 (2011), 91-109.

[45] C. Y. Chun, Q. Z. Huan, R. Z.Yu"DSSC with a novel Pt counter electrodes using pulsed electroplating techniques" **Current Applied Physics**, 11 (2011), 147-153.

[46] D. A. H. Hanaor and Charles C. Sorrell "Review of the anatase to rutile phase transformation" **Journal of Material Science**, 46 (2011), 855–874.

[47] C. Lu and Z. Chen "Anodic aluminum oxide base-Nanostructures and Devices" **Encyclopedia of Nanoscience and Nanotechnology**, 11 (2011), 235-259.

[48] A. Mutalib Md Jani, D. Losic, N. H. Voelcker "Nanoporous anodic aluminium oxide: Advances in surface engineering and emerging applications" **Progress in Materials Science**, 58 (2013), 636-704.

[49] N. Han and J. C. Ho "One-Dimensional Nanomaterials for Energy Applications" Their synthesis-structure-property relationships and applications*"* **Nanocrystalline Materials (Second Edition)**, 2014, Pages 75-120.

[50] T. Lee, H. Sue, and X. Cheng, "Solid-state dye-sensitized solar cells based on ZnO nanoparticle and nanorod array hybrid photoanodes", **Nanoscale Research Letters**, 6 (2011), 517.

[51] T. Oekermann, D. Zhang, T. Yoshida and H. Minoura, "Electron Transport and Back Reaction in Nanocrystalline TiO_2 Films Prepared by Hydrothermal Crystallization" **Journal of Physic Chemistry B**, 108 (2004), 2227-2235.

LIST OF PUBLICATION

Publication

[1] M. Nukunudompanich, S. Chuangchote, J. Wootthikanokkhan, Y. Suzuki, "TiO_2 Nanorods Prepared from Anodic Aluminum Oxide Template and their Applications in Dye-Sensitized Solar Cells", International Letters of Chemistry, Physics and Astronomy, Vol 46, pp. 30-36, Jan. 2015.

[2] M. Nukunudompanich, S. Chuangchote, Y. Okamoto, Y. Shinoda and Y. Suzuki "TiO_2 Nanorods and Semi-nanotubes Prepared from Anodic Aluminum Oxide Template and Their Applications as Photoelectrodes in Dye-Sensitized Solar Cells" Journal Ceramic Society of Japan., 123 [5] 428-432 (2015).

Awarded

[1] Awarded "IWP2014 PRIZE"at "International Workshop on Science and Patents 2014 (University Hall, University of Tsukuba) September 9, 2014"

APPENDIX

A1. Photovoltaic properties of a conventional DSSC

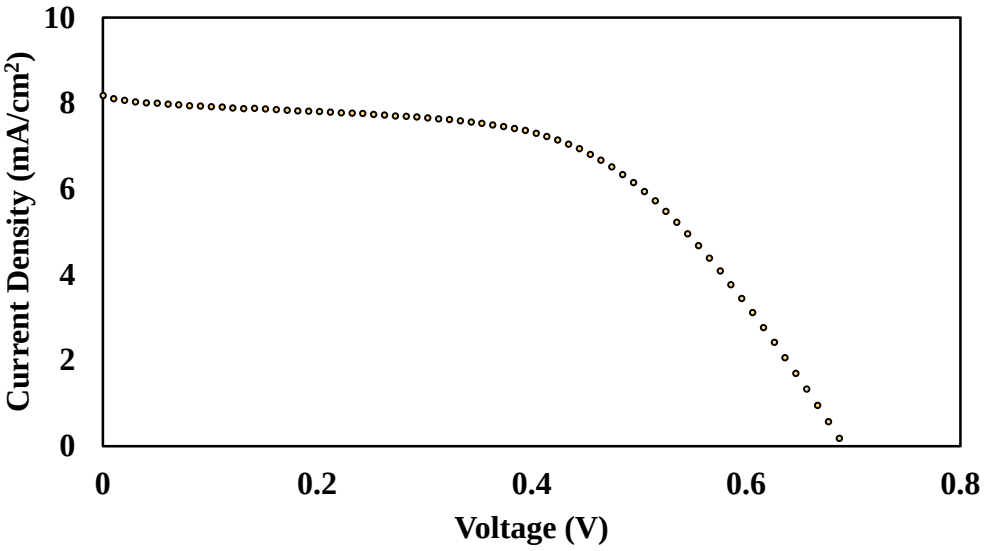

Fig. A.1 *J-V* characteristics of a DSSC fabricated from conventional pristine P25 TiO_2 nanoparticles.

Table A.2 PCE of conventional DSSC.

Sample (TiO_2 P25)	J_{sc} (mA/cm^2)	V_{oc} (V)	FF	Efficiency (%)	Area (cm^2)
TiO_2	2.52	0.64	0.56	0.91	1.17

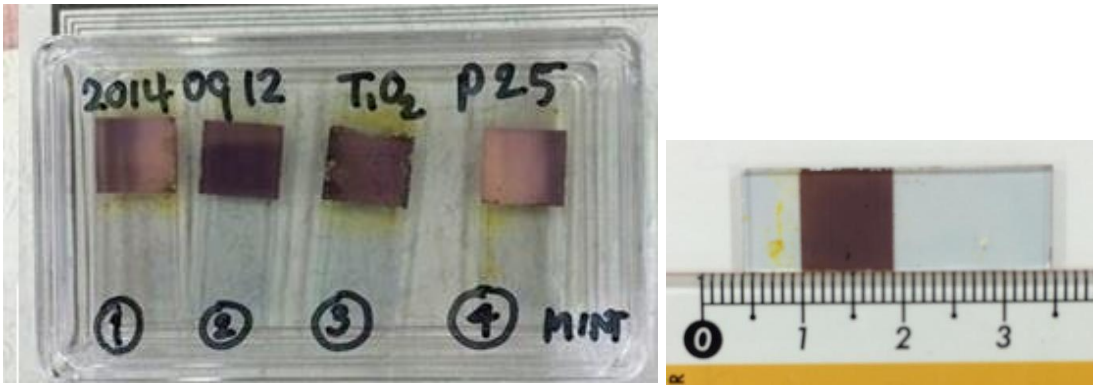

Fig. A.2. Photographical images of opened cell samples and size of samples.

A2. Photovoltaic properties of conventional DSSCs

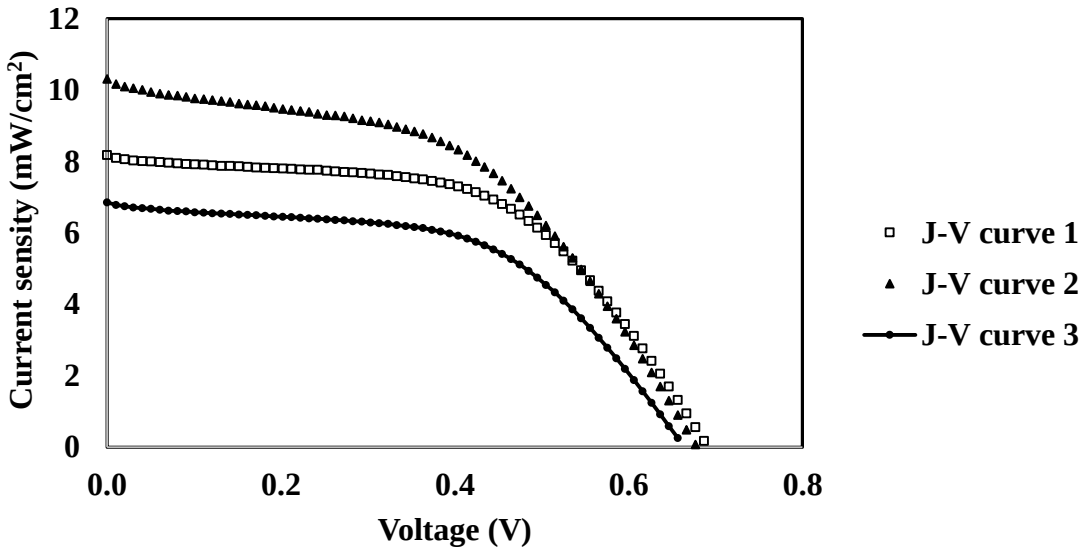

Fig. A.4 *J-V* characteristics of DSSCs fabricated from conventional pristine P25 TiO_2 nanoparticles.

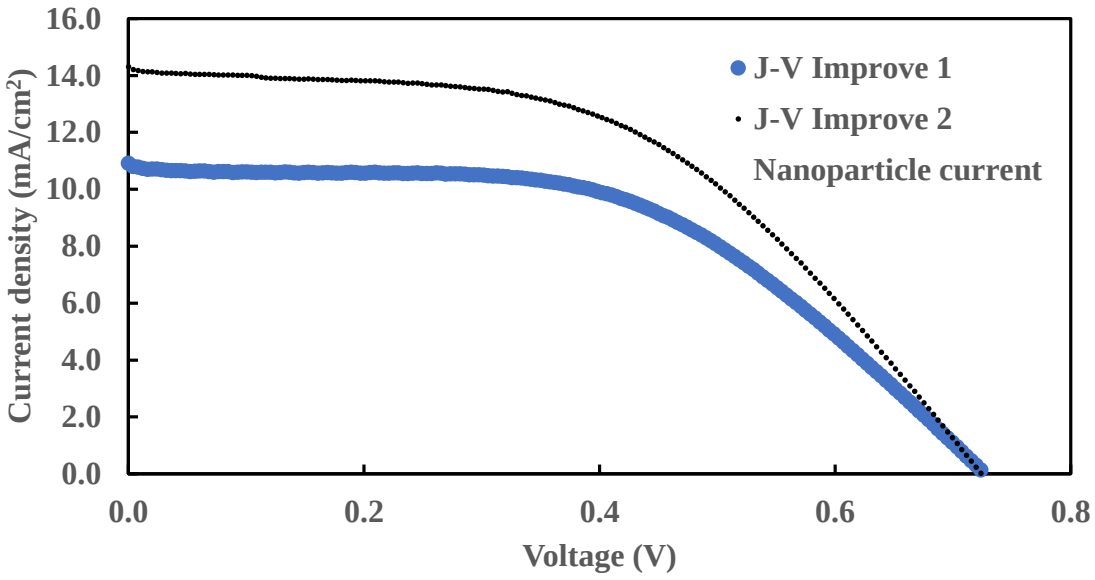

Fig. A.5 *J-V* characteristics of DSSCs fabricated from improved pristine P25 cells (the 1st time of experiment).

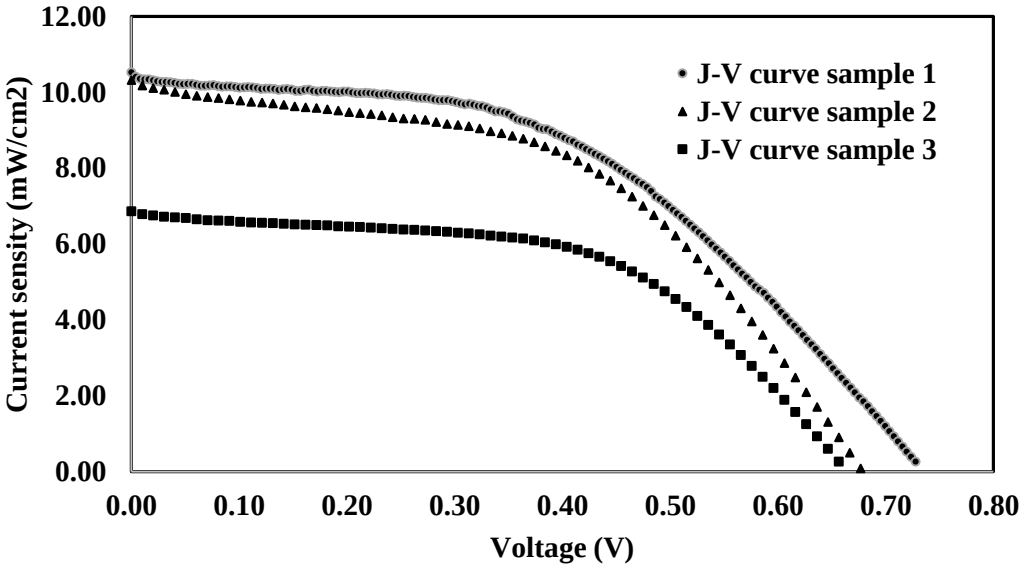

Fig. A.6 *J-V* characteristics of DSSCs fabricated from improved pristine P25 cells (the 2nd time of experiment).

Table A.2 Comparison PCEs of conventional and improved DSSCs.

Sample (TiO_2 P25)	J_{sc} (mA/cm^2)	V_{oc} (V)	FF	Efficiency (%)	Area (cm^2)
Conventional					
1	8.19	0.697	0.544	3.10	0.9
2	10.03	0.687	0.481	3.41	0.9
4	6.86	0.697	0.514	2.46	0.9
Improved					
1	10.43	0.687	0.521	5.12	0.88
2	10.92	0.727	0.520	4.13	0.95
3	11.43	0.708	0.444	3.59	1.00

A3. SEM Images

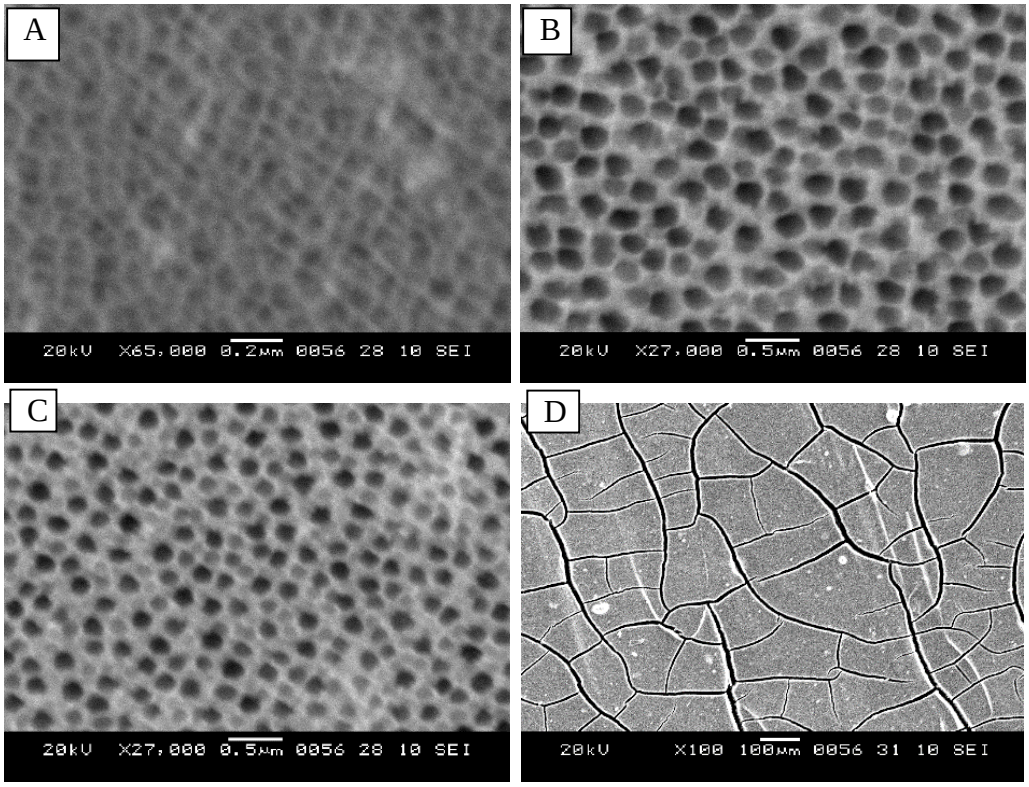

Fig. A.7 SEM images of (A) surface side of AAO template (100 nm), (B) backside of AAO template, (C) surface side of AAO (20 nm), and (D) surface of coated dye on P25.

A4. Improved DSSCs

Table A.3 Comparison of DSSCs made of P25 TiO_2 nanoparticles and P25 TiO_2 nanoparticles mixed with nanorods fabricated from AAO template via immersion setting (IS). The mixing ratio was 10:95 and 15:85.

Sample	J_{sc} (mA/cm^2)	V_{oc} (V)	*FF*	*PCE* (%)	Area (cm^2)
Ref. P25 TiO_2	10.92	0.73	0.52	4.13	0.95
RM 2 1	8.302	0.719	0.57	3.41	0.99
RM 2 2	9.389	0.704	0.56	3.72	0.96
RM 2 3	7.431	0.719	0.59	3.17	1.01
Repeated RM 2	9.885	0.729	0.58	4.19	1.03
1	10.52	0.719	0.56	4.25	1.01
Repeated RM 2	10.89	0.714	0.56	4.33	0.98
2	9.628	0.704	0.55	3.76	1.01
Repeated RM 2	10.35	0.709	0.53	3.92	0.96
3	9.817	0.699	0.55	3.74	0.98
RM 3 1					
RM 3 2					
RM 3 3					

*RM = Random mixing of TiO_2 nanorods achieved from 100 nm pore diameter AAO template via IS and P25 TiO_2. Numbers after RM are numbers of layers of mixed nanorods/P25 and pristine P25.

Note: all of samples were controlled fabrication process at same conditions.

Table A.4 Comparison of PCEs of conventional DSSCs and random mixing ratio between SNT/NP (5:95, mass fraction)

Sample	J_{sc} (mA/cm^2)	V_{oc} (V)	*FF*	Efficiency (%)
Layer 1 TiO_2 nanoparticles	10.92	0.73	0.52	4.13
Layer 1 SNT/NP	10.94	0.71	0.51	4.00
Layer 1 SNT/NP:Layer 2 SNT/NP	11.72	0.70	0.51	4.20
Layer 1 NP:Layer 2 SNT/NP	12.82	0.70	0.48	4.27

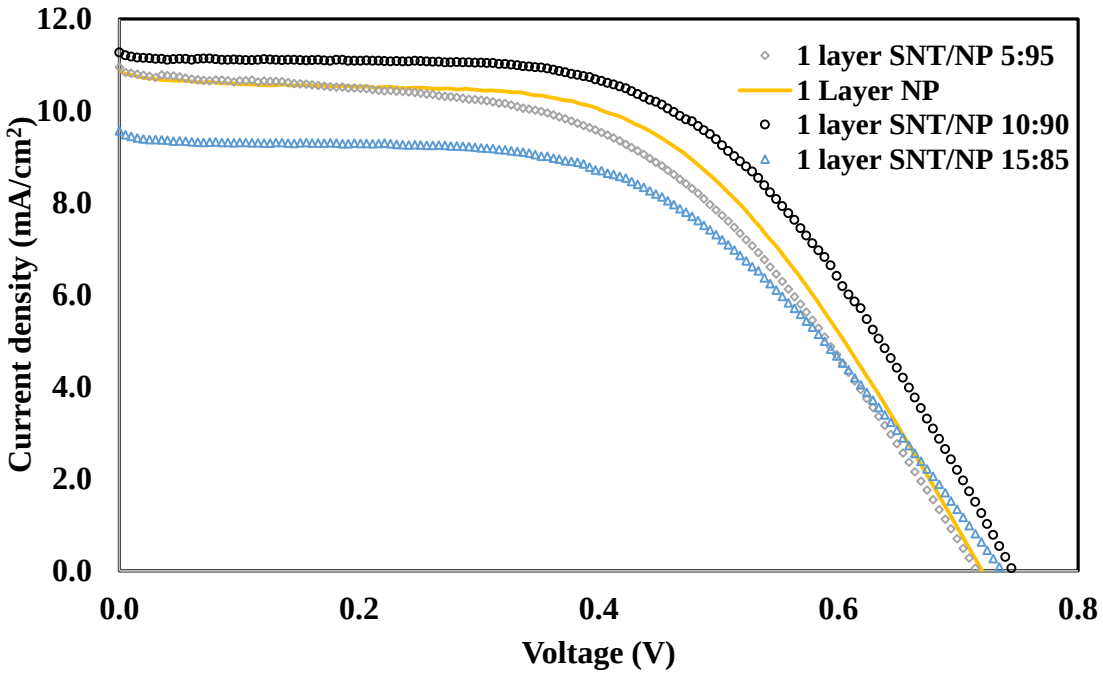

Fig. A.8 *J-V* characteristics of DSSCs fabricated from pristine P25 compared with mixed TiO_2 semi-nanotube/nanoparticle at a ratio of 5:95, 10:90, and 15:85 (by weight) with 1-layer coating.

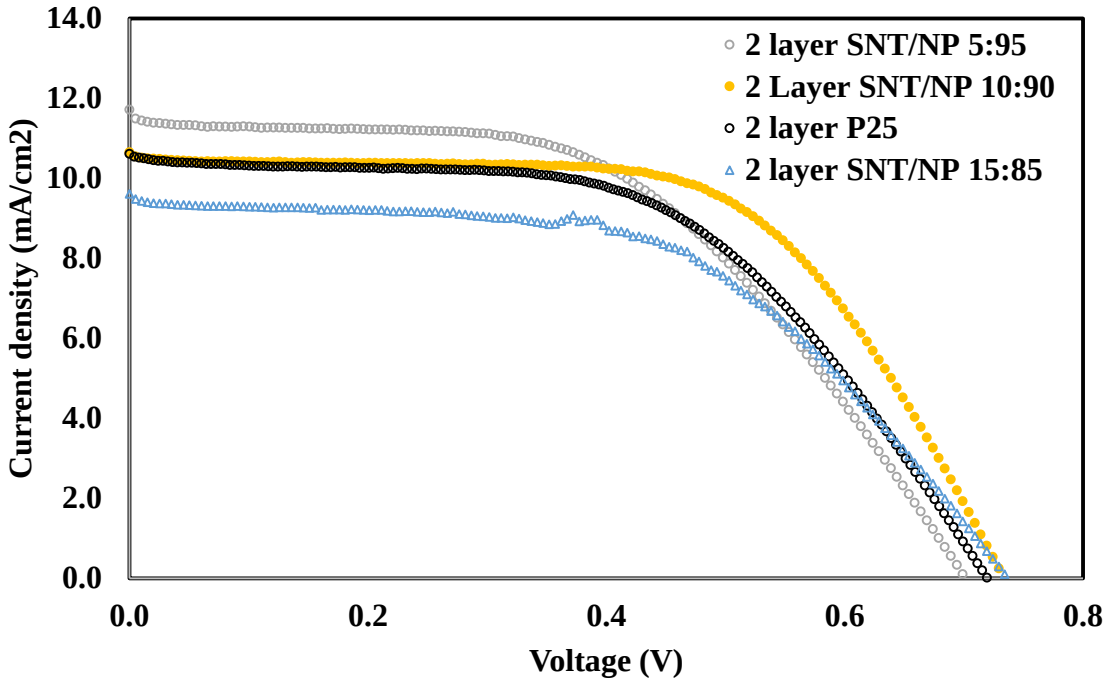

Fig. A.9 *J-V* characteristics of DSSCs fabricated from pristine P25 compared with mixed TiO_2 semi-nanotube/nanoparticle at a ratio of 5:95, 10:90, and 15:85 (by weight) with 2-layer coating.

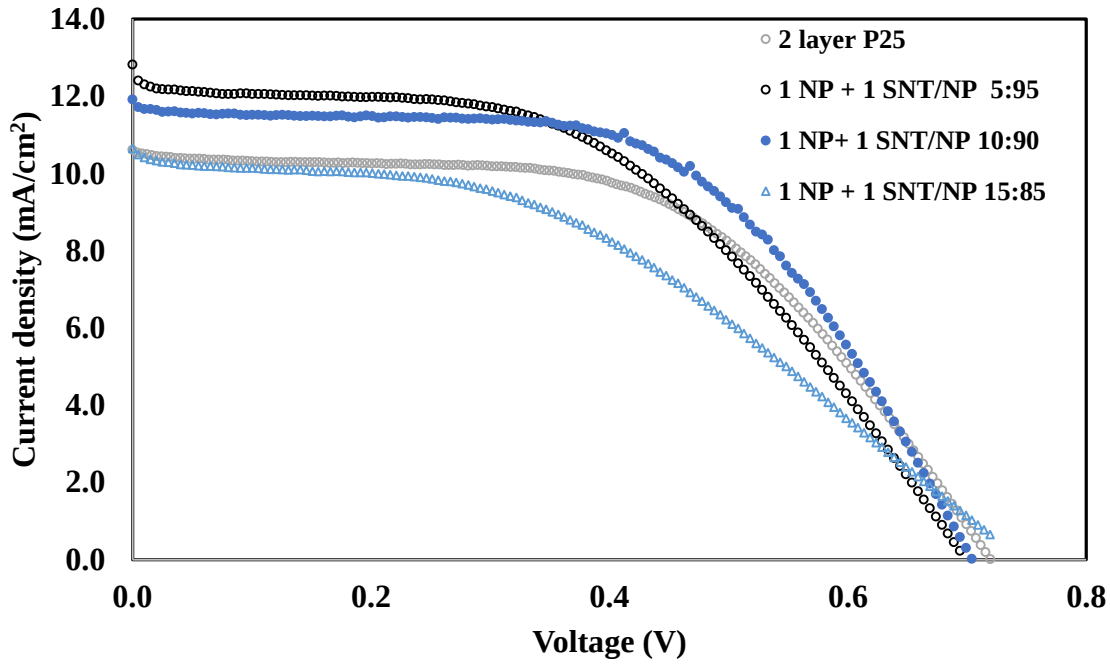

Fig. A.10 *J-V* characteristics of DSSCs fabricated from pristine P25 compared with mixed TiO_2 semi-nanotube/nanoparticle at a ratio of 5:95, 10:90, and 15:85 (by weight) with 2-layer coating.